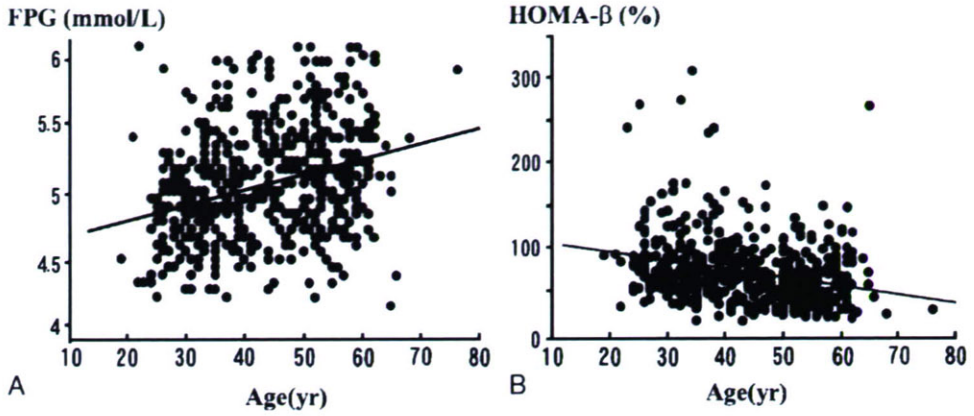

Fig. 1. Distribution of FPG (A) and HOMA-β (B) cell by age. The FPG increases with age ($r = 0.30$, $P < .0001$). The HOMA-β cell is negatively correlated with age ($r = 0.24$, $P < .0001$).

$P < .0001$, respectively). Multiple regression analysis shows that both BMI and TG are independently associated with HOMA-IR (standardized $\beta = 0.41$ and 0.15, respectively). Body mass index was the strongest determinant of HOMA-IR, and BMI did not increase with age significantly in Japanese men ($r = 0.07$, not significant).

3.4. Analysis of 3 subgroups of NFG subjects

To evaluate the factors involved in increasing FPG in Japanese NFG and the ADA recommendation of lowering the threshold of upper limit of normal FPG from 6.1 to 5.6 mmol/L [16], we divided our NFG subjects into 3 subgroups: low FPG (FPG <5.0 mmol/L), high FPG ($5.0 \leq$ FPG < 5.6 mmol/L), and mild impairment of fasting glucose (mild IFG) ($5.6 \leq$ FPG < 6.1 mmol/L); and age, BMI, TG, and insulin secretion and sensitivity were compared. As shown in Table 2, high FPG and mild IFG have higher age and BMI than low FPG (both $P < .0001$). Insulin in high FPG and mild IFG is increased compared with that in low FPG ($P < .001$); insulin in mild IFG is similar to that in high FPG. The HOMA-IR in high FPG and mild IFG is increased compared with that in low FPG ($P < .0001$). The HOMA-β in high FPG and mild IFG is decreased compared with that in low FPG ($P < .0001$); the HOMA-β in mild IFG is decreased compared with that in high FPG ($P < .001$).

4. Discussion

In this study, we analyzed the factors responsible for age-related elevation of FPG in Japanese men with NFG. Fasting plasma glucose was found to increase with age primarily because of reduced β-cell function rather than increased insulin resistance. In addition, we have elucidated that there was no compensatory increase in insulin secretion in mild IFG (FPG 5.6-6.1 mmol/L).

Our study subjects were composed only of men because the number of female subjects was 158, which is not comparable with male subjects. Some reports showed a difference between men and women in the elevation of FPG [24-26], and another showed similar results between men and women in the elevation of FPG [27]. We analyzed the results from our 158 female subjects, and we could not find

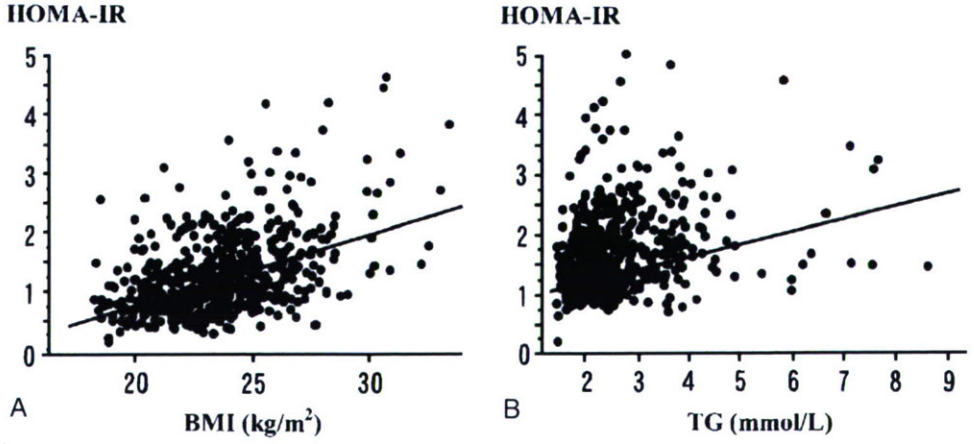

Fig. 2. Distribution of HOMA-IR by BMI (A) and TG (B). Both BMI and TG are associated with HOMA-IR (BMI: $r = 0.49$, $P < .0001$; TG: $r = 0.33$, $P < .0001$).

Table 2
Comparison of 3 FPG subgroups of NFG subjects

	Low FPG (FPG <5.0 mmol/L)	High FPG (5.0 ≤ FPG < 5.6 mmol/L)	Mild IFG (5.6 ≤ FPG < 6.1 mmol/L)
n	268	288	101
Age (y)	42.0 ± 0.7	45.7 ± 0.6[a]	49.8 ± 1.0[a, b]
BMI (kg/m^2)	23.0 ± 0.2	23.9 ± 0.1[a]	24.3 ± 0.3[a]
TC (mmol/L)	5.07 ± 0.05	5.23 ± 0.05[c]	5.35 ± 0.08[d]
TG (mmol/L)	1.30 ± 0.05	1.55 ± 0.06[d]	1.56 ± 0.09[c]
HDL-C (mmol/L)	1.45 ± 0.02	1.44 ± 0.02	1.45 ± 0.03
F-IRI (μU/mL)	4.6 ± 0.2	5.7 ± 0.2[a]	5.6 ± 0.3[e]
HOMA-IR	0.96 ± 0.04	1.31 ± 0.04[a]	1.44 ± 0.07[a]
HOMA-β (%)	78.5 ± 3.1	65.2 ± 1.9[a]	49.2 ± 2.4[a, b]

Data are mean ± SE.
[a] $P < .0001$ vs low FPG.
[b] $P < .001$ vs high FPG.
[c] $P < .05$ vs low FPG.
[d] $P < .005$ vs low FPG.
[e] $P < .0005$ vs low FPG.

remarkable differences with male subjects (data not shown). Further studies are necessary to elucidate the sex difference of the factors responsible for elevation of FPG. Although some reports showed an increase in insulin resistance in subjects older than 70 years, our male subjects were younger than 70 years. Insulin resistance in subjects older than 70 years was reported mainly because of the change in abdominal adiposity [28,29]; and in representative epidemiologic studies such as the Funagata study and the Hisayama study, the mean age of developing glucose intolerance is around 50 years in Japanese [21-23]. For these reasons, our subjects being around the age of 50 years was enough for our purpose in this study of elucidating the factors responsible for FPG elevation from normal to borderline glucose dysregulation.

Fasting plasma glucose increased by 0.011 mmol/L per year, in accord with previous reports [30]. The HOMA-β decreased by 0.85% per year, clearly indicating reduced basal insulin secretion. Although previous studies in whites and in other populations have found that insulin resistance is closely associated with age-related FPG elevation [12,31], HOMA-IR did not increase with age significantly in our subjects. To characterize the insulin resistance of our study population, we performed both simple and multiple regression analyses between HOMA-IR and the other measured factors. The BMI and serum TG levels were strongly associated with HOMA-IR ($P < .0001$), in accord with our previous results in Japanese diabetic patients [32]. Although BMI was the strongest determinant of HOMA-IR, it did not increase with age; the mean BMI of 23.6 kg/m^2 is in accord with Japanese statistical data [21-23] and is much lower than in whites [33,34]. The BMI of Asians in other studies is also reported to be lower, suggesting a common metabolic profile [35]. The leaner Japanese subjects in this study might therefore be expected to be less influenced by insulin resistance in comparison with whites.

Impaired fasting glycemia is a prediabetic state characterized by FPG elevation without increased 2h-PG. We previously reported that insulin secretory capacity and insulin sensitivity are both already decreased in IFG [8-10], suggesting the clinical importance of early deterioration of β-cell function and insulin sensitivity in developing prediabetes. In addition, we regarded the PG level of 5.6 mmol/L as an important FPG threshold value according to ADA recommendation [16]. Therefore, we compared insulin secretion and insulin sensitivity in 3 subgroups of NFG subjects: low FPG (FPG <5.0 mmol/L), high FPG (5.0 ≤ FPG < 5.6 mmol/L), and mild IFG (5.6 ≤ FPG < 6.1 mmol/L). Insulin secretion in mild IFG was not increased compared with that in high FPG, indicating impaired compensatory insulin secretion against increasing insulin resistance. Some reports have found that early-phase insulin secretion and insulin sensitivity are both decreased in NGT at a higher range of FPG (FPG >5.1-5.3 mmol/L) [36-38]. Fortunately, we could analyze 56 subjects during the 8-year follow-up period using oral glucose tolerance test results [39]. The subjects who developed from NFG to IFG showed decreasing insulin sensitivity and insulin secretory capacity, and those who developed from NFG to IGT showed decreased early insulin secretory response. These follow-up data were compatible with our previous data of IFG and IGT [5,8,10,39]. Taken together, these data indicate that insulin secretory capacity is already decreased in NGT at the higher range of FPG and that a lack of compensatory insulin secretion appears at greater than 5.6 mmol/L in FPG.

We find in Japanese NFG subjects that age-related FPG elevation is mainly due to decreased β-cell function rather than to increasing insulin resistance as in white subjects. In addition, analysis of 3 degrees of increasing FPG indicates that failure of compensatory insulin secretion is responsible for the elevation in FPG in these subjects. Thus, these data could be helpful in reconsideration of the threshold FPG for prediabetes to be recommended by the ADA [16]. However, decreasing the upper threshold of FPG entails increasing the IFG population, a costly social health problem [40]. Further studies are required to clarify the ethnic differences in the development of diabetes and diabetic complications and the value of clinical interventions in newly diagnosed IFG patients.

Acknowledgment

This study was supported in part by Health Sciences Research Grants for Comprehensive Research on Aging and Health; Research on Health Technology Assessment; and Research on Human Genome, Tissue Engineering, and Food Biotechnology from the Ministry of Health, Labour, and Welfare, and by Leading Project of Biostimulation from the Ministry of Education, Culture, Sports, Science, and Technology, Japan. We thank Use Techno, Ono Pharmaceutical, ABBOTT JAPAN, and Dainippon Pharmaceutical for their help in the study.

References

[1] Porte Jr D. Banting lecture 1990. Beta-cells in type II diabetes mellitus. Diabetes 1991;40:166-80.

[2] Lillioja S, Mott DM, Spraul M, et al. Insulin resistance and insulin secretory dysfunction as precursors of non–insulin-dependent diabetes mellitus. Prospective studies of Pima Indians. N Engl J Med 1993;329: 1988-92.

[3] DeFronzo RA. Lilly lecture 1987. The triumvirate: beta-cell, muscle, liver. A collusion responsible for NIDDM. Diabetes 1988;37:667-87.

[4] Mandavilli A, Cyranoski D. Asia's big problem. Nat Med 2004;10: 325-7.

[5] Fukushima M, Suzuki H, Seino Y. Insulin secretion capacity in the development from normal glucose tolerance to type 2 diabetes. Diabetes Res Clin Pract 2004;66:S37-43.

[6] Alberti KG, Zimmet PZ. Definition, diagnosis and classification of diabetes mellitus and its complications. Part 1: diagnosis and classification of diabetes mellitus provisional report of a WHO consultation. Diabet Med 1998;15:539-53.

[7] Suzuki H, Fukushima M, Usami M, et al. Factors responsible for development from normal glucose tolerance to isolated postchallenge hyperglycemia. Diabetes Care 2003;26:1211-5.

[8] Fukushima M, Usami M, Ikeda M, et al. Insulin secretion and insulin sensitivity at different stages of glucose tolerance: a cross-sectional study of Japanese type 2 diabetes. Metabolism 2004;53:831-5.

[9] Nishi Y, Fukushima M, Suzuki H, et al. Insulin secretion and insulin sensitivity in Japanese subjects with impaired fasting glucose and isolated fasting hyperglycemia. Diabetes Res Clin Pract 2005;70: 46-52.

[10] Izuka M, Fukushima M, Taniguchi A, et al. Factors responsible for glucose intolerance in Japanese subjects with impaired fasting glucose. Horm Metab Res 2007;39:41-5.

[11] Wiener K, Roberts NB. Age does not influence levels of HbA1c in normal subject. QJM 1999;92:169-73.

[12] Chang AM, Halter JB. Aging and insulin secretion. Am J Physiol Endocrinol Metab 2003;284:E7-E12.

[13] Paolisso G, Tagliamonte MR, Rizzo MR, et al. Advancing age and insulin resistance: new facts about an ancient history. Eur J Clin Invest 1999;29:758-69.

[14] Coon PJ, Rogus EM, Drinkwater D, et al. Role of body fat distribution in the decline in insulin sensitivity and glucose tolerance with age. J Clin Endocrinol Metab 1992;75:1125-32.

[15] Kuroe A, Fukushima M, Usami M, et al. Impaired beta-cell function and insulin sensitivity in Japanese subjects with normal glucose tolerance. Diabetes Res Clin Pract 2003;59:71-7.

[16] Report of the expert committee on the diagnosis and classification of diabetes mellitus. Diabetes Care 2003;26:S5-S20.

[17] Taniguchi A, Fukushima M, Sakai M, et al. Remnant-like particle cholesterol, triglycerides, and insulin resistance in nonobese Japanese type 2 diabetic patients. Diabetes Care 2000;23:1766-9.

[18] Bonora E, Targher G, Alberiche M, et al. Homeostasis model assessment closely mirrors the glucose clamp technique in the assessment of insulin sensitivity: studies in subjects with various degrees of glucose tolerance and insulin sensitivity. Diabetes Care 2000;23:57-63.

[19] Matthews DR, Hosker JP, Rudenski AS, et al. Homeostasis model assessment: insulin resistance and beta-cell function from fasting plasma glucose and insulin concentrations in man. Diabetologia 1985; 28:412-9.

[20] Fukushima M, Taniguchi A, Sakai M, et al. Homeostasis model assessment as a clinical index of insulin resistance. Comparison with the minimal model analysis. Diabetes Care 1999;22:1911-2.

[21] Ohmura T, Ueda K, Kiyohara Y, et al. The association of the insulin resistance syndrome with impaired glucose tolerance and NIDDM in the Japanese general population: the Hisayama study. Diabetologia 1994;37:897-904.

[22] Tominaga M, Eguchi H, Manaka H, et al. Impaired glucose tolerance is a risk factor for cardiovascular disease, but not impaired fasting glucose. The Funagata diabetes study. Diabetes Care 1999;22:920-4.

[23] Ministry of Health, Labour and Welfare Statistical database: Statistics and Information Department, second edition, chapter 1 "Public health "

[24] Williams JW, Zimmet PZ, Shaw JE, et al. Gender differences in the prevalence of impaired fasting glycaemia and impaired glucose tolerance in Mauritius. Does sex matter? Diabet Med 2003;20:915-20.

[25] Schianca GP, Castello L, Rapetti R, et al. Insulin sensitivity: gender-related differences in subjects with normal glucose tolerance. Nutr Metab Cardiovasc Dis 2006;16:339-44.

[26] Rutter MK, Parise H, Benjamin EJ, et al. Impact of glucose intolerance and insulin resistance on cardiac structure and function: sex-related differences in the Framingham Heart Study. Circulation 2003;107: 448-54.

[27] Yates AP, Laing I. Age-related increase in haemoglobin A1c and fasting plasma glucose is accompanied by a decrease in beta cell function without change in insulin sensitivity: evidence from a cross-sectional study of hospital personnel. Diabet Med 2002;19:254-8.

[28] DeNino WF, Tchernof A, Dionne IJ, et al. Contribution of abdominal adiposity to age-related differences in insulin sensitivity and plasma lipids in healthy nonobese women. Diabetes Care 2001;24:925-32.

[29] Bryhni B, Jenssen TG, Olafsen K, et al. Age or waist as determinant of insulin action? Metabolism 2003;52:850-7.

[30] Bando Y, Ushiogi Y, Okafuji K, et al. The relationship of fasting plasma glucose values and other variables to 2-h postload plasma glucose in Japanese subjects. Diabetes Care 2001;24:1156-60.

[31] Utzschneider KM, Carr DB, Hull RL, et al. Impact of intra-abdominal fat and age on insulin sensitivity and beta-cell function. Diabetes 2004; 53:2867-72.

[32] Taniguchi A, Fukushima M, Sakai M, et al. The role of the body mass index and triglyceride levels in identifying insulin-sensitive and insulin-resistant variants in Japanese non–insulin-dependent diabetic patients. Metabolism 2000;49:1001-5.

[33] Kuczmarski MF, Kuczmarski RJ, Najjar M. Effects of age on validity of self-reported height, weight, and body mass index: findings from the Third National Health and Nutrition Examination Survey, 1988-1994. J Am Diet Assoc 2001;101:28-34.

[34] Flegal KM, Carroll MD, Ogden CL, et al. Prevalence and trends in obesity among US adults, 1999-2000. JAMA 2002;288:1723-7.

[35] Qiao Q, Nakagami T, Tuomilehto J, et al. Comparison of the fasting and the 2-h glucose criteria for diabetes in different Asian cohorts. Diabetologia 2000;43:1470-5.

[36] Piche ME, Arcand-Bosse JF, Despres JP, et al. What is a normal glucose value? Differences in indexes of plasma glucose homeostasis in subjects with normal fasting glucose. Diabetes Care 2004;27:2470-7.

[37] Sato Y, Komatsu M, Katakura M, et al. Diminution of early insulin response to glucose in subjects with normal but minimally elevated fasting plasma glucose. Evidence for early beta-cell dysfunction. Diabet Med 2002;19:566-71.

[38] Godsland IF, Jeffs JA, Johnston DG. Loss of beta cell function as fasting glucose increases in the non-diabetic range. Diabetologia 2004; 47:1157-66.

[39] Mitsui R, Fukushima M, Nishi Y. Factors responsible for deteriorating glucose tolerance in newly diagnosed type 2 diabetes in Japanese men. Metabolism 2006;55:53-8.

[40] Genuth S, Alberti KG, Bennett P, et al. Follow-up report on the diagnosis of diabetes mellitus. Diabetes Care 2003;26:3160-7.

Am J Physiol Endocrinol Metab 294: E61–E68, 2008.
First published October 30, 2007; doi:10.1152/ajpendo.00358.2007.

A novel GIP receptor splice variant influences GIP sensitivity of pancreatic β-cells in obese mice

Norio Harada,[1] Yuichiro Yamada,[1] Katsushi Tsukiyama,[1] Chizumi Yamada,[1] Yasuhiko Nakamura,[1] Eri Mukai,[1,2] Akihiro Hamasaki,[1] Xibao Liu,[1] Kentaro Toyoda,[1] Yutaka Seino,[1,3] and Nobuya Inagaki[1,4]

[1]*Department of Diabetes and Clinical Nutrition, Kyoto University Graduate School of Medicine, Kyoto;* [2]*Japan Association for the Advancement of Medical Equipment, Tokyo;* [3]*Kansai Electric Power Hospital, Osaka; and* [4]*Core Research for Evolutional Science and Technology of Japan Science and Technology, Kyoto, Japan*

Submitted 11 June 2007; accepted in final form 11 October 2007

Harada N, Yamada Y, Tsukiyama K, Yamada C, Nakamura Y, Mukai E, Hamasaki A, Liu X, Toyoda K, Seino Y, Inagaki N. A novel GIP receptor splice variant influences GIP sensitivity of pancreatic β-cells in obese mice. *Am J Physiol Endocrinol Metab* 294: E61–E68, 2008. First published October 30, 2007; doi:10.1152/ajpendo.00358.2007.— Gastric inhibitory polypeptide (GIP) is an incretin that potentiates insulin secretion from pancreatic β-cells by binding to GIP receptor (GIPR) and subsequently increasing the level of intracellular adenosine 3′,5′-cyclic monophosphate (cAMP). We have identified a novel GIPR splice variant in mouse β-cells that retains intron 8, resulting in a COOH-terminal truncated form (truncated GIPR). This isoform was coexpressed with full-length GIPR (wild-type GIPR) in normal GIPR-expressing tissues. In an experiment using cells transfected with both GIPRs, truncated GIPR did not lead to cAMP production induced by GIP but inhibited GIP-induced cAMP production through wild-type GIPR ($n = 3$–4, $P < 0.05$). Wild-type GIPR was normally located on the cell surface, but its expression was decreased in the presence of truncated GIPR, suggesting a dominant negative effect of truncated GIPR against wild-type GIPR. The functional relevance of truncated GIPR in vivo was investigated. In high-fat diet-fed obese mice (HFD mice), blood glucose levels were maintained by compensatory increased insulin secretion ($n = 8$, $P < 0.05$), and cAMP production ($n = 6$, $P < 0.01$) and insulin secretion ($n = 10$, $P < 0.05$) induced by GIP were significantly increased in isolated islets, suggesting hypersensitivity of the GIPR. Total GIPR mRNA expression was not increased in the islets of HFD mice, but the expression ratio of truncated GIPR to total GIPR was reduced by 32% compared with that of control mice ($n = 6$, $P < 0.05$). These results indicate that a relative reduction of truncated GIPR expression may be involved in hypersensitivity of GIPR and hyperinsulinemia in diet-induced obese mice.

gastric inhibitory polypeptide; gastric inhibitory polypeptide receptor; alternative splicing; dominant negative effect; obesity

OBESITY LEADS TO INSULIN RESISTANCE, characterized by fasting hyperinsulinemia and excessive insulin secretion after meal ingestion in the attempt to maintain euglycemia (25). Obesity is an important risk factor in progression to type 2 diabetes mellitus (14) and also in cardiovascular disease (16), and reduction of obesity can normalize hyperinsulinemia and impede the progression of diabetes and arteriosclerosis.

Incretins are a group of peptide hormones released from the gastrointestinal tract into the circulation in response to meal ingestion that potentiate glucose-stimulated insulin secretion and include gastric inhibitory polypeptide (GIP), also called glucose-dependent insulinotropic polypeptide (24). GIP is secreted from the K cells of the duodenum and proximal jejunum upon meal ingestion and binds to the GIP receptor (GIPR) on the surface of pancreatic β-cells, adipose tissues, and osteoblasts to stimulate insulin secretion (21), fat accumulation (20), and bone formation (30) by increasing the level of intracellular adenosine 3′,5′-cyclic monophosphate (cAMP).

Previously, we found that GIPR-deficient mice exhibit insufficient compensatory insulin secretion upon high-fat loading (21), indicating that GIP plays a critical role in maintaining the blood glucose level by inducing hypersecretion of insulin in diet-induced obesity. Increased GIP signaling in obesity might be due to hypersecretion of GIP from K cells or hypersensitivity of GIPR to GIP at the β-cells. An increased blood GIP level in obesity has been reported in some studies (3, 6) but is controversial (27, 28), and altered GIPR sensitivity in obesity has not been investigated.

GIPR is the G protein-coupled receptor (GPCR) that belongs to the secretin-vasoactive intestinal peptide receptor family (31, 33). The gene encoding the human GIPR contains 14 exons (33); the rat and mouse GIPR-encoding genes contain 15 exons (2, 21). Alternative splicing is a frequent occurrence in the transcriptome in higher eukaryotic cells and can alter the structure of the encoded protein and dramatically increase the efficiency of the proteome in regulating cell function. In the present study, we report a novel splice variant GIPR expressed in mouse pancreatic β-cells and the investigation of its functional significance in hypersensitivity of GIPR in high-fat diet-induced obese mice.

MATERIALS AND METHODS

Animals. Male C57BL/6 mice (7 wk old) were obtained from Shimizu (Kyoto, Japan). The animals were fed control fat chow (CFD; 10% fat, 20% protein, and 70% carbohydrate by energy) or high-fat chow (HFD; 45% fat, 20% protein, and 35% carbohydrate by energy) for 10 wk. The energy density of both diets was 3.57 kcal/g. After a 16-h fast, oral glucose tolerance tests (OGTTs) (2 g/kg body wt) were performed in CFD and HFD mice. Blood glucose and plasma insulin levels were measured in samples taken at the indicated times. Blood glucose levels were determined by the glucose oxidase method. Plasma insulin levels were determined using enzyme immunoassay (Shibayagi, Gumma, Japan). Animal care and procedures were approved by the Animal Care Committee of Kyoto University.

Address for reprint requests and other correspondence: Y. Yamada, Dept. of Internal Medicine, Div. of Endocrinology, Diabetes, and Geriatric Medicine, Akita University School of Medicine, 1-1-1, Hondo, Akita 010-8543, Japan (e-mail: yamada@gipc.akita-u.ac.jp).

The costs of publication of this article were defrayed in part by the payment of page charges. The article must therefore be hereby marked "*advertisement*" in accordance with 18 U.S.C. Section 1734 solely to indicate this fact.

0193-1849/08 $8.00 Copyright © 2008 the American Physiological Society

Downloaded from ajpendo.physiology.org on February 28, 2008

Isolation and measurement of GIPR mRNA. Total RNA was extracted from tissues (pancreatic islets, proximal jejunum, and adipose tissues) of C57/BL6 mice and Wistar rats (Shimizu) and mouse pancreatic β-cell line MIN6 cells with RNeasy mini kit (Qiagen, Valencia, CA). Islets were isolated by collagenase digestion (29). The extracted RNA was treated with DNase (Qiagen), and the cDNA was prepared by reverse transcription (Superscript II; Invitrogen, Grand Island, NY) with an oligo(dT) primer. To detect mouse full-length GIPR, COOH-terminal and NH_2-terminal primers of GIPR were designed as follows: forward, 5-CTTTTCAAGGATGCCCCTGCGGTTGC-3′; reverse, 5′-CCTTTACCTAGCAGTAACTTTTCCAAGA-3. The cDNA was amplified through 35 cycles with denaturation at 96°C for 15 s, annealing at 60°C for 30 s, and extension at 72°C for 2 min. To clearly detect splice variants of GIPR, a pair of GIPR primers was designed as follows: mouse GIPR forward, 5-CTGCCTGCCGCACGGCCCAGAT-3′; reverse, 5′-CAAATGGCTTTGACTTCGTTG-3; rat GIPR forward, 5′-CTGCCTGCCGCACAGCCCAGAT-3′; reverse, 5′- CAAATGGCTTTGACTTCGTTG -3′. The cDNA was amplified through 40 cycles with denaturation at 95°C for 15 s, annealing at 55°C for 15 s, and extension at 72°C for 30 s. The PCR products were fractioned on 2% agarose gels. Negative controls of cDNAs of tissues were prepared in the absence of reverse transcriptase at the reverse transcription step.

GIPR mRNA levels in the islets were measured by quantitative RT-PCR using ABI PRISM 7000 Sequence Detection System (Applied Biosystems, Foster City, CA). The mouse sequences of forward and reverse primers to evaluate total GIPR expression were 5′-CCTCCACTGGGTCCCTACAC-3′ and 5′-GATAAACACCCTCCACCAGTAG-3′, respectively, whereas the sequences of forward and reverse primers to evaluate truncated GIPR expression were 5′-CCTACCCCGTGGAACCAG-3′ and 5′-GTGGTGGGGAGCCAAGAT-3′, respectively. SYBR Green PCR Master Mix (Applied Biosystems) was prepared for PCR run. The thermal cycling conditions were denaturation at 95°C for 10 min followed by 50 cycles at 95°C for 15 s and 60°C for 1 min. Total GIPR mRNA levels were corrected for GAPDH (Applied Biosystems) mRNA levels.

Plasmid construction. The cDNA fragments of mouse wild-type GIPR, truncated GIPR, and $G_s\alpha$ protein were obtained from mouse (C57BL/6) islets by RT-PCR. The cDNA fragment of wild-type GIPR was cloned into pCMV-6c vector and pFLAG-CMV-5b vector (wild-type GIPR-FLAG; Sigma, St. Louis, MO). The cDNA fragment of truncated GIPR was cloned into pCMV-6c vector and pAcGFP-N1 vector (truncated GIPR-GFP; Takara, Tokyo, Japan). The two GIPR constructs were FLAG- or green fluorescent protein (GFP)-tagged at the COOH terminus. The cDNA fragment of mouse $G_s\alpha$ protein was cloned into pCMV-6c vector.

Cell culture and transfection. COS-7 cells were seeded in 10-cm dishes and cultured in Dulbeco's modified Eagle's medium supplemented with 10% fetal bovine serum. Expression plasmids of wild-type GIPR, truncated GIPR, wild-type GIPR-FLAG, and truncated GIPR-GFP were transfected into COS-7 cells using FuGENE 6 transfection reagent (Roche, Basel, Switzerland). Plasmid (5 μg/well) was diluted into serum-free medium, and FuGENE 6 reagent was added and incubated at room temperature for 30 min. After incubation, the mixture was added to COS-7 cells.

Measurement of intracellular cAMP level in GIPR-expressing COS-7 cells. COS-7 cells were transfected with the wild-type GIPR expression plasmid and the truncated GIPR expression plasmid using the amounts indicated in figure legends, passaged after 24 h into 12-well plates (1×10^5 cells/well), and cultured for an additional 48 h. The cells were washed twice with phosphate-buffered saline (PBS), and the reaction was started in 0.5 ml of Krebs-Ringer bicarbonate buffer (KRBB) containing 0.1 mM 3-isobutyl-1-methylxanthine (IBMX) with various concentrations of mouse GIP (provided by Sanwakagaku Kenkyusho, Mie, Japan) and then incubated at 37°C for 30 min. Incubation buffers were removed and the cells lysed by addition of 0.1 M HCl (0.5 ml/well) to each well (15). Plates were incubated at room temperature for 15 min with gentle rotation. The samples were centrifuged for 10 min at 600 *g*. cAMP levels were measured by enzyme immunoassay (cAMP low pH EIA kit; R&D Systems, Minneapolis, MN). Data were expressed as the increment with GIP treatment from basal cAMP levels.

Fluorescence microscopy. Immunofluorescence staining was performed using COS-7 cells either transfected with the wild-type GIPR-FLAG expression plasmid (2 μg) or the truncated GIPR-GFP expression plasmid (2 μg) or cotransfected with the two plasmids (1 μg each) with $G_s\alpha$ protein expression plasmid (2 μg). We used $G_s\alpha$ protein expression plasmid for structural stability of wild-type GIPR on plasma membrane (11). The cells were cultured on coverslips for 72 h, washed twice with PBS, and treated with acetone-methanol (1:1) for 4 min. After being washed sequentially with PBS containing 1% bovine serum albumin (BSA), the cells were incubated at room temperature for 24 h with anti-GFP monoclonal mouse antibody (Sigma) and anti-FLAG polyclonal rabbit antibody (Sigma) or anti-calnexin rabbit polyclonal antibody (Stressgen, San Diego, CA) in PBS containing 1% BSA. After being washed three times with PBS, the cells were immunostained at room temperature for 1 h using Cy3-conjugated anti-rabbit IgG (Sigma) or Alexa fluor 488 anti-mouse IgG (Molecular Probes, Eugene, OR) (23). Fluorescent images were analyzed using a confocal laser microscope LSM510 Meta (Carl Zeiss, Heidelberg, Germany).

Binding assay. Binding assay was performed using COS-7 cells either transfected with the wild-type GIPR expression plasmid (1 μg) or the truncated GIPR expression plasmid (1 μg) or cotransfected with the two plasmids (1 μg each) (total amount of plasmid DNA used for transfection was adjusted to 5 μg by adding pCMV-6c vector). After 72 h of incubation the cells were washed twice with PBS, and the collected cells were incubated with ^{125}I-labeled GIP (50,000 counts/min; Amersham Biosciences, Piscataway, NJ) in 1 ml of buffer containing 50 mM Tris (pH 7.4), 0.2 mM sucrose, 5 mM $MgCl_2$, and 1 mg/ml bacitracin at 22°C for 1 h in the absence or presence of 10^{-6} M nonradioactive GIP. Samples were filtered through Whatman GF/C filters (24 mm) and rapidly washed three times with ice-cold PBS. The radioactivity of the filters was measured in a γ-counter (22). Competitive binding assay was also performed using COS-7 cells transfected with the wild-type GIPR expression plasmid (1 μg) or cotransfected with the two plasmids (1 μg each). Various concentrations of nonradioactive GIP, ranging from 10^{-12} to 10^{-6} M, were used as competitors. Specific binding of radioactive GIP was calculated by subtracting binding of radioactive GIP in the presence of nonradioactive GIP. Protein content was measured by Bradford method. Data were expressed as specific binding to each of the GIPR-expressing cells after subtraction of the specific binding to cells transfected with pCMV-6c vector.

Immunoprecipitation and Western blot analysis. We performed Western blot analysis using COS-7 cells either transfected with the wild-type GIPR-FLAG expression plasmid (2 μg) or the truncated GIPR-GFP expression plasmid (2 μg) or cotransfected with the two plasmids (1 μg each). After 72 h of incubation, the collected cells were washed twice with PBS containing protease inhibitor (Complete; Roche) and suspended in 1 ml of PBS containing protease inhibitor. The cells were homogenized and centrifuged at 800 *g* for 5 min. The supernatant was centrifuged at 10,000 *g* for 10 min. The supernatant was further centrifuged at 100,000 *g* for 30 min to separate the endoplasmic reticulum (ER)-enriched fraction and the supernatant. The ER-enriched fraction was solubilized in 1 ml of PBS containing protease inhibitor and 2% Triton X-100 on ice for 15 min and centrifuged at 15,000 *g* for 10 min. The supernatant was incubated at 4°C for 2 h with mixing for immunoprecipitation using anti-FLAG M2 affinity beads (Sigma). The beads collected by centrifugation were washed three times with 1 ml PBS containing protease inhibitor, suspended in 20 μl of sample buffer (0.2 M Tris, 10% sucrose, 10% SDS, and 5 mM EDTA), and incubated at 98°C for 5 min. After centrifugation, the supernatants were electrophoresed through 5–16%

Downloaded from ajpendo.physiology.org on February 28, 2008

polyacrylamide gradient gels. The gels were subjected to immunoblotting using anti-FLAG polyclonal rabbit antibody (Sigma) or anti-GFP polyclonal rabbit antibody (Sigma) and anti-rabbit or anti-mouse IgG horseradish peroxdase-linked antibody (Amersham Biosciences). The immunoblots were visualized by electrochemiluminescence (Amersham Biosciences).

To determine whether the two GIPRs insert into the ER membrane, the ER-enriched fraction of COS-7 cells cotransfected with the two plasmids (1 μg each) were incubated in PBS containing 0.2 M sucrose in the absence or presence of 0.1 M Na_2CO_3 (pH 10.5) for 1 h on ice. After centrifugation at 100,000 *g* for 30 min, Western blot was performed with the supernatant and pellet using an antibody against FLAG or GFP.

Measurement of insulin secretion and intracellular cAMP production in isolated islets. Islets were isolated from mice and handpicked under a microscope. For insulin secretion studies, groups of 10 islets were preincubated at 37°C for 30 min in KRBB containing 2.8 mM glucose and 0.2% BSA and gassed with 95% O_2 and 5% CO_2. The islets were incubated at 37°C for 30 min in 0.5 ml of KRBB

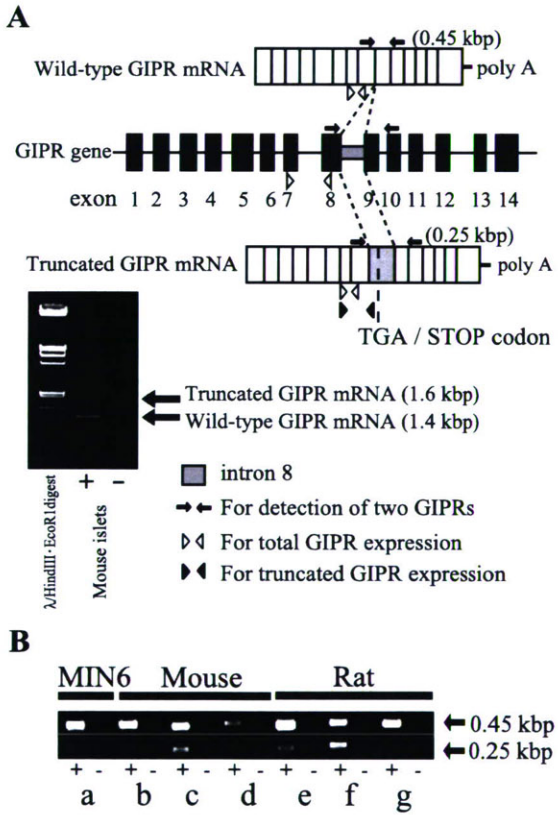

Fig. 1. Structure and expression of the splice variant gastric inhibitory polypeptide (GIP) receptor (GIPR). *A*: the structure of 2 splice variant GIPRs. PCR amplification of mouse (C57BL/6) islet cDNA was performed using COOH-terminal and NH_2-terminal primers of GIPR. The upper band (1.6 kbp) encodes a truncated GIPR isoform that retained the sequence of intron 8 (0.2 kbp) during RNA processing. The lower band (1.4 kbp) encodes wild-type GIPR isoform (full-length GIPR). A minus lane is negative control of mouse islet. The specific primer pair was designed to clearly detect 2 bands of GIPR by RT-PCR (arrows). The primer pair for quantitative RT-PCR to analyze total GIPR expression and truncated GIPR expression is indicated as open arrowhead and filled arrowhead, respectively. Intron 8 is indicated as gray box. *B*: tissue distribution of truncated GIPR in mice, rats, and MIN6 cells. The 0.25-kbp band shows the amplified DNA fragment of wild-type GIPR; the 0.45-kbp band shows that of truncated GIPR. cDNA was prepared from mouse (*a–d*) and rat (*e–f*) tissues, and RT-PCR was performed (*a*, MIN6 cells; *b* and *e*, adipose tissue; *c* and *f*, islets; *d* and *g*, proximal jejunum). A minus lane is negative control of each tissue.

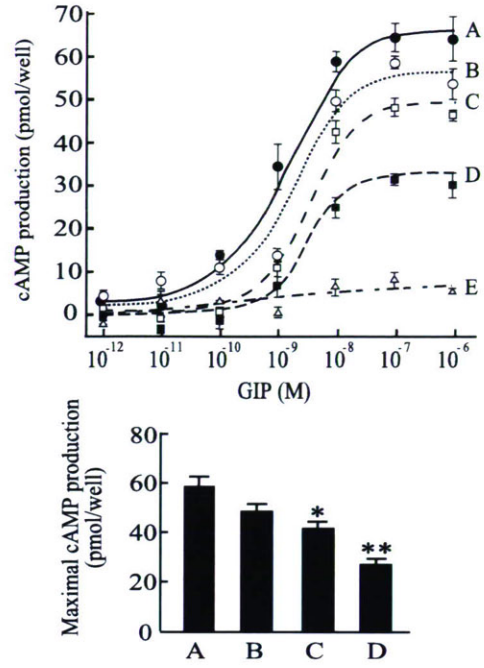

Fig. 2. Dose response analysis of GIP-induced cAMP production in GIPR-expressing COS-7 cells. *Top*: the ratios of the 2 GIPRs were as follows: wild-type GIPR expression plasmid DNA (μg) to truncated GIPR expression plasmid DNA (μg) = 1:0 (●; *A*), 1:0.5 (○; *B*), 1:1 (■; *C*), 1:2 (□; *D*), and 0:1 (△; E). The total amount of plasmid DNA used for each transfection was adjusted to 5 μg by adding pCMV-6c vector. Values are means ± SE. *Bottom*: cAMP induced by 10^{-6} M GIP is shown (n = 3–4). All ED_{50} values of GIP response curves were ~3.0 nM. Values are means ± SE. *$P < 0.05$; **$P < 0.01$ vs. cAMP induction of wild-type GIPR expression.

containing 2.8 mM or 11.1 mM glucose and 0.2% BSA in the absence or presence of high potassium (30 mM KCl). The islets were also incubated at 37°C for 30 min in 0.5 ml of KRBB containing 11.1 mM glucose and 0.2% BSA with or without mouse GIP (10^{-9} or 10^{-7} M) or 5 μM forskolin. Aliquots of the sample buffer were subjected to RIA assay for insulin. To determine insulin content, the islets were homogenized in 0.4 ml acid-ethanol and extracted at 4°C overnight. The acidic extracts were dried and subjected to insulin measurement.

For cAMP production studies, 20 preincubated islets were incubated at 37°C for 30 min in 0.3 ml of KRBB containing 11.1 mM glucose, 0.2% BSA, 1 mM IBMX, and 10 mM HEPES (pH 7.4) with or without 10^{-9} M GIP, 10^{-7} M GIP, or 5 μM forskolin. The incubation was stopped by the addition of 60 μl of 2 M $HClO_4$. The samples were immediately mixed and sonicated in ice-cold water for 4 min. The samples were centrifuged for 4 min at 3,000 *g*, and aliquots (240 μl) were neutralized by 60 μl of 1 M Na_2CO_3 and diluted with 60 μl of 2 M HEPES (pH 7.4). cAMP levels were measured by EIA assay.

Statistical analysis. Values are expressed as means ± SE. Statistical analyses were performed using ANOVA and unpaired student's *t*-test. *P* values <0.05 were considered significant.

RESULTS

Identification of truncated GIPR. PCR amplification and sequencing of full-length GIPR from mouse islet cDNA revealed expression of two isoforms (Fig. 1*A*). The upper band (1.6 kbp) is characterized by unsplicing of intron 8 (0.2 kbp). As a result of the addition, the predicted amino acid reading frame is shifted within the region encoding transmembrane domain 4 and an in-frame stop codon is produced, generating a COOH-terminal truncated form of 263 amino acids desig-

Downloaded from ajpendo.physiology.org on February 28, 2008

nated as truncated GIPR. The lower band (1.4 kbp) corresponds to full-length GIPR of 460 amino acids designated as wild-type GIPR. To estimate truncated GIPR expression in different tissues, RT-PCR was performed using a different detection primer pair (Fig. 1*B*). Truncated GIPR was expressed not only in mouse islets but also in mouse proximal jejunum and adipose tissue. Truncated GIPR was also expressed in a mouse pancreatic β-cell line (MIN6), rat islets, proximal jejunum, and adipose tissue.

Function of truncated GIPR. To determine the functional properties of truncated GIPR, COS-7 cells were transfected with wild-type and truncated GIPR expression plasmid separately and stimulated with GIP (Fig. 2). In wild-type GIPR-expressing cells, GIP increased cAMP levels in a concentration-dependent manner. In contrast, GIP failed to stimulate cAMP induction in truncated GIPR-expressing cells. COS-7 cells were then cotransfected with wild-type and truncated GIPR expression plasmids. As the amount of truncated GIPR expression plasmid was increased from 0.5 to 2 μg in the presence of 1 μg of wild-type GIPR expression plasmid, maximal cAMP production induced by GIP was reduced, indicating that truncated GIPR had a dominant negative effect against wild-type GIPR. We examined whether truncated GIPR influenced glucagon-like peptide-1 (GLP-1)-induced cAMP production using GLP-1 receptor-expressing COS-7 cells. GLP-1-induced cAMP production was not decreased in the presence of truncated GIPR (data not shown), indicating that the dominant negative effect of truncated GIPR is specific to GIPR.

To determine how truncated GIPR affects wild-type GIPR in COS-7 cells, we constructed a COOH-terminal FLAG-tagged wild-type GIPR expression plasmid (wild-type GIPR-FLAG) and a COOH-terminal GFP-tagged truncated GIPR expression plasmid (truncated GIPR-GFP). When each of these expression plasmids was transfected into COS-7 cells (Fig. 3*A*, *a* and *b*), wild-type GIPR-FLAG was expressed on the cell surface

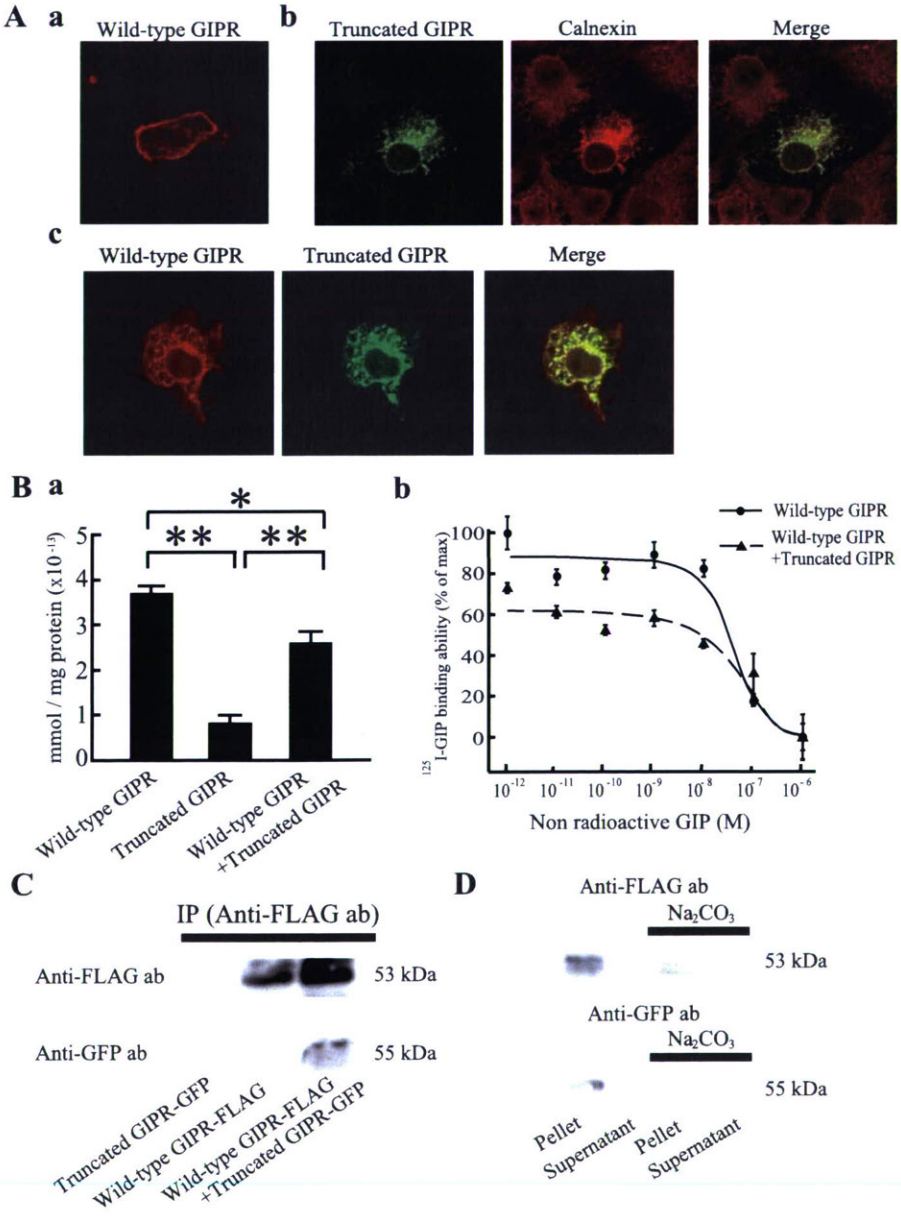

Fig. 3. Cellular localization and interaction of wild-type GIPR and truncated GIPR in GIPR-expressing COS-7 cells. *A*: immunofluorescence staining of the GIPR-expressing COS-7 cells. COS-7 cells were transfected with wild-type GIPR-FLAG (*a*) or truncated GIPR-green fluorescent protein (GFP) (*b*). To estimate localization of truncated GIPR-GFP, anti-calnexin antibody was used as endoplasmic reticulum (ER) maker (green, truncated GIPR-GFP; red, calnexin; yellow, merge). Cotransfection of the 2 GIPRs (*c*) was performed (red, wild-type GIPR-FLAG; green, truncated GIPR-GFP; yellow, merge). Localization of the GIPRs was analyzed by dual wavelength confocal microscopy. We repeated these experiments using 1×10^5 cells 3 times. *B*: binding assay analysis using GIPR-expressing COS-7 cells ($n = 4$; *a*). Competitive GIP binding curves using COS-7 cells transfected with wild-type GIPR (●) or cotransfected with two GIPRs (▲) (wild-type GIPR to truncated GIPR = 1:1 μg, $n = 5$; *b*). The IC_{50} values of binding curves were 5.6×10^{-8} and 7.2×10^{-8} M, respectively. Data are expressed as specific binding to each of the GIPR-expressing cells after subtraction of the specific binding to cells transfected with pCMV-6c vector. Values are means ± SE. $^*P < 0.05$; $^{**}P < 0.01$. *C*: immunoprecipitation and Western blot analysis of ER-enriched fractions of GIPR-expressing COS-7 cells. Immunoprecipitation was performed using anti-FLAG M2 affinity beads. Wild-type GIPR was detected in COS-7 cells transfected with wild-type GIPR alone and cotransfected with the 2 GIPRs using anti-FLAG polyclonal antibody. Truncated GIPR was detected only in COS-7 cells cotransfected with the 2 GIPRs using anti-GFP polyclonal antibody. *D*: Western blot analysis of ER-enriched fractions of the 2 GIPRs-expressing COS-7 cells with or without Na_2CO_3 treatment.

Downloaded from ajpendo.physiology.org on February 28, 2008

whereas truncated GIPR-GFP expression was limited to the ER, as resolved by anti-calnexin antibody. When both wild-type GIPR-FLAG and truncated GIPR-GFP were coexpressed in COS-7 cells (Fig. 3*A*, *c*), the expression of wild-type GIPR-FLAG on the cell surface decreased and remained highly within the ER. To determine whether the tags of the receptor influenced receptor trafficking, we constructed tag-changed plasmids [a COOH-terminal GFP-tagged wild-type GIPR expression plasmid (wild-type GIPR-GFP) and a COOH-terminal FLAG-tagged truncated GIPR expression plasmid (truncated GIPR-FLAG)] and transfected them into COS-7 cells. Truncated GIPR-FLAG also was located in the ER and decreased wild-type GIPR-GFP trafficking from the ER to the cell membrane (data not shown). We performed a GIP binding assay using COS-7 cells transfected with nontagged wild-type and truncated GIPR. The GIP binding ability of wild-type GIPR was significantly decreased in the presence of truncated GIPR (Fig. 3*B*, *a*). Analysis of GIP binding curves by performing a competitive binding assay showed similar IC_{50} values of both curves (Fig. 3*B*, *b*).

Immunoprecipitation was performed on the prepared ER-enriched fractions of COS-7 cells transfected with the two GIPRs to determine whether truncated GIPR interacts with wild-type GIPR (Fig. 3*C*). In the ER-enriched fraction of cotransfected cells, immunoreactive truncated GIPR-GFP could be detected after immunoprecipitation with the FLAG-tagged wild-type GIPR, indicating that truncated GIPR interacts with wild-type GIPR on the ER membrane. Western blot analysis was performed using the ER-enriched fraction treated by Na_2CO_3 to determine whether the two GIPRs are inserted into the ER membrane (Fig. 3*D*). With Na_2CO_3 treatment peripheral membrane proteins are solubilized into the buffer, whereas integral membrane proteins are insoluble. Two GIPRs were detected in the pellet of the ER-enriched fraction untreated by Na_2CO_3. The two GIPRs were also detected in the pellet of the ER-enriched fraction treated by Na_2CO_3, indicating that the two GIPRs are stably inserted into the ER membrane. Thus, truncated GIPR influenced trafficking of wild-type GIPR from the ER to the cell surface by interacting with wild-type GIPR in the ER.

GIPR sensitivity in islets of HFD mice. To analyze the functional significance of truncated GIPR in vivo, we investigated GIPR sensitivity of β-cells in obese mice induced by high-fat diet. Mice were fed high-fat chow or control fat chow for 10 wk. Body weight was significantly higher in HFD mice compared with CFD mice (37.9 ± 1.8 and 32.3 ± 0.83 g, respectively, $P < 0.05$). To determine the effect of high-fat diet on glucose homeostasis, we carried out OGTTs. Blood glucose levels were similar in HFD and CFD mice (Fig. 4*A*). We then measured plasma insulin levels at the indicated times during OGTTs. Plasma insulin levels were twofold higher in HFD mice at 15 min (1.4 ± 0.2 and 2.7 ± 0.3 ng/ml, respectively, $P < 0.05$), and the area under the curve of insulin secretion during OGTT was significantly increased in HFD mice compared with CHD mice (191.6 ± 21.2 and 130.8 ± 15.8 $ng \cdot ml^{-1} \cdot min^{-1}$, respectively, $P < 0.05$) (Fig. 4*B*). These results suggest compensatory hyperinsulinemia in an attempt to maintain blood glucose levels in high-fat diet-induced obese mice.

To determine sensitivity to GIP in the islets of HFD mice, GIP-induced insulin secretion from isolated islets of these mice

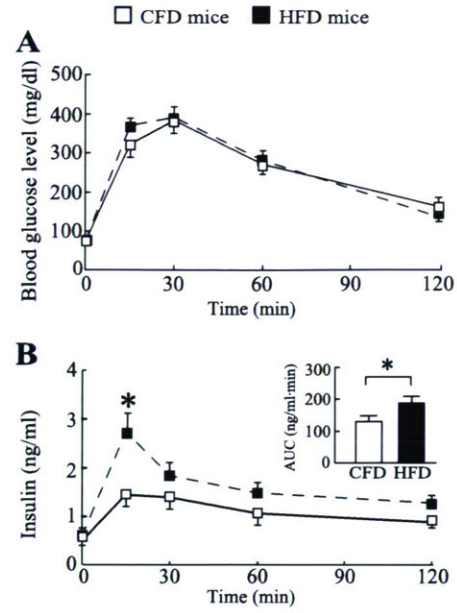

Fig. 4. Oral glucose tolerance tests (OGTTs) in control fat chow (CFD) and high-fat chow (HFD) mice. *A*: blood glucose levels during OGTTs in CFD (□) and HFD (■) mice ($n = 8$). *B*: plasma insulin levels during OGTTs in CFD (□) and HFD (■) mice ($n = 8$). Area under the curves of the insulin secretion during OGTTs in CFD mice (open bar) and HFD mice (filled bar) were also represented. Values are means ± SE. $^*P < 0.05$ vs. CFD mice.

was examined in the presence of 11.1 mM glucose, in which incretin can potentiate insulin secretion. Insulin secretion stimulated by 11.1 mM glucose was similar in the islets of CHD and HFD mice (Fig. 5*A*). The islets of HFD mice showed significantly increased insulin secretion in response to 10^{-9} or 10^{-7} M GIP compared with those of CFD mice. On the other hand, forskolin, an adenylate-cyclase activator, increased insulin secretion in islets of CFD and HFD mice to a similar extent. In the presence of 2.8 and 11.1 mM glucose, insulin secretion stimulated by high potassium (30 mM) was also similar in the islets of CFD and HFD mice, respectively (Table. 1). The insulinotropic effect of GIP requires an increase in the level of intracellular cAMP in theβ-cells, and cAMP production in the islets of HFD mice was significantly higher than that in CFD mice in the presence of GIP (Fig. 5*B*). However, forskolin increased intracellular cAMP production in the islets of CFD and HFD mice to a similar extent. Thus, GIPR sensitivity to GIP was increased specifically in the islets of HFD mice.

Expression of total and truncated GIPR in islets of HFD mice. To confirm differences in GIPR expression in islets between HFD and CFD mice, quantitative RT-PCR was performed. Total GIPR expression in the islets of HFD mice was similar to that of CFD mice (Fig. 6*A*). The relative expression level of truncated GIPR was then compared in the islets of HFD and CFD mice. The ratio of truncated GIPR to total GIPR expression in the islets of HFD mice was decreased by 32% compared with that in CFD mice (Fig. 6*B*).

DISCUSSION

In the present study, we have identified a novel splice variant GIPR expressed in mouse pancreatic β-cells and characterized its effect on GIPR sensitivity in high-fat diet-induced obese mice.

Downloaded from ajpendo.physiology.org on February 28, 2008

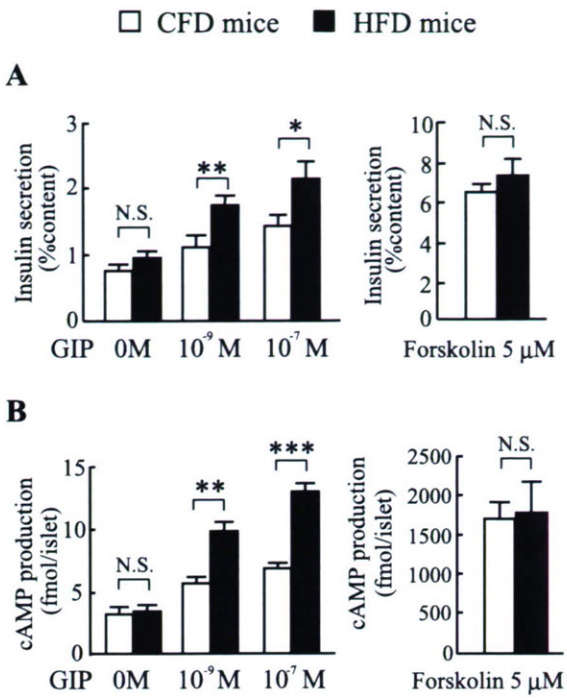

Fig. 5. Insulin secretion and cAMP production induced by GIP in isolated islets of CFD and HFD mice.Insulin secretion (n = 10; A) and intracellular cAMP levels (n = 6; B) in isolated islets of CFD (open bars) and HFD mice (filled bars) were examined in response to 10^{-9} or 10^{-7} M GIP in the presence of 11.1 mM glucose. The isolated islets of these mice were incubated with 5 μM forskolin to assess maximal insulin secretion and cAMP production. Values are means ± SE. *$P < 0.05$, **$P < 0.01$, and ***$P < 0.001$ vs. CFD mice.

We (21) previously investigated GIP-induced insulin secretion using *GIPR*$^{-/-}$ mice under high-fat feeding. The plasma insulin levels after meal ingestion were increased in high-fat diet-fed *GIPR*$^{+/+}$ mice compared with those in control diet-fed *GIPR*$^{+/+}$ mice, resulting in similar glucose levels. However, the postprandial glucose levels were increased by the lack of GIP-induced compensatory insulin secretion in high-fat diet-fed *GIPR*$^{-/-}$ mice, suggesting that increased insulin secretion due to enhanced GIP signaling is required to maintain glucose homeostasis in the obese state. In the present study, we have demonstrated hypersensitivity of GIPR to GIP in β-cells of high-fat-induced obese mice. Increased sensitivity of GIPR to GIP might result from increased expression of GIPR or hypersensitivity of intracellular GIP signal transduction. Some (9, 18) studies have reported that GIPR expression is an important factor in altering the GIP sensitivity of β-cells. In the study of diabetic Zucker fatty rats, GIPR mRNA expression and protein

Table 1. *Insulin secretion induced by glucose and high potassium (30 mM KCl) in the isolated islets of CFD and HFD mice*

%Content	CFD Mice	HFD Mice	*P* Value
2.8 mM glucose	0.69±0.21	0.68±0.07	NS
2.8 mM glucose + high potassium	0.99±0.12	1.00±0.17	NS
11.1 mM glucose	1.12±0.14	1.22±0.10	NS
11.1 mM glucose + high potassium	2.14±0.25	2.42±0.34	NS

Values are means ± SE; CFD (mice fed control fat chow; n = 5–6) vs. HFD mice (mice fed high-fat chow; n = 5–6). NS, not significant.

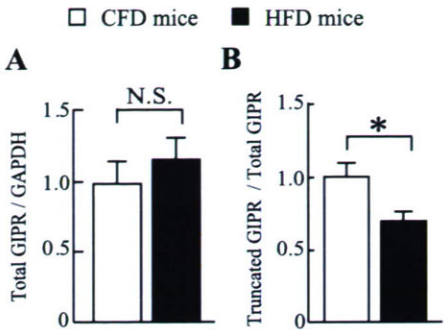

Fig. 6. Total and truncated GIPR expression in islets of CFD and HFD mice. Quantitative RT-PCR of total GIPR (A) and truncated GIPR (B) were assessed in islets of CFD (n = 6) and HFD mice (n = 6). The ratio of truncated GIPR to total GIPR (B) was calculated by quantitative RT-PCR of total GIPR and truncated GIPR. The data on HFD mice are shown relative to CFD mice. Values are means ± SE. *$P < 0.05$ vs. CFD mice.

were decreased in islets compared with that of lean rats, which led to diminished GIPR sensitivity to GIP (17). Here, we found that total GIPR expression was not decreased and that GIPR sensitivity to GIP was increased in isolated islets of our HFD mice due to decreased expression of truncated GIPR, in contrast to the findings in diabetic obese rats. Our HFD mice were mild obese and mild hyperinsulinemia induced by high-fat feeding rather than by genetic factors. In addition, our obese mice did not have diabetes. Thus, differences of the expression of GIPR and subsequent GIPR sensitivity to GIP may be due to the different phenotypes of diabetic obese rats and HFD mice.

We had previously obtained the extra band of this GIPR variant as well as the band of wild-type GIPR when we amplified mouse islet cDNA to detect wild-type GIPR using NH_2-terminal and COOH-terminal primers of GIPR. We analyzed the cDNA sequence of the extra band and identified it as a splice variant of GIPR that was not produced by PCR error. Indeed, certain GIPR splice variants resulting in truncation have been reported in previous studies (7, 32). These splice variants were detected from cDNA libraries of human islets and insulinoma. However, the variants were not examined in regard to their regulatory role in GIPR sensitivity. In the present study, by evaluating the function of truncated GIPR in transfected COS-7 cells, we have shown that truncated GIPR has a dose-dependent dominant negative effect against wild-type GIPR.

GPCRs were generally thought to function as monomers, but recent studies (5, 12, 13) have reported that GPCRs can form homodimeric or heterodimeric complexes with receptors in the ER and that these complexes are important in receptor folding and trafficking to the plasma membrane. In the present study, we investigated the mechanism of negative action of truncated GIPR against wild-type GIPR function using immunochemistry and immunoprecipitation of cotransfected cells. Truncated GIPR interacted with wild-type GIPR in the ER and influenced wild-type receptor trafficking to the cell membrane. Some GPCRs have specific motifs for dimerization that are required for transport of the receptors from the ER to the cell surface (1, 8, 19, 26). Mutations in these motifs prevent dimerization with wild-type receptors and inhibit their trafficking to the cell membrane, indicating a dominant negative effect against the wild-type receptor (19, 26). Although these specific motifs are

Downloaded from ajpendo.physiology.org on February 28, 2008

not found in GIPR, truncated GIPR might have formed from complexes with wild-type GIPR in our experiments.

To evaluate the functional relevance of truncated GIPR in vivo, we investigated the expression of truncated GIPR in β-cells. The relative abundance of truncated GIPR expression was decreased in islets of HFD mice. The decreased dominant negative effect due to reduced expression of truncated GIPR might well be involved in augmented intracellular cAMP production and insulin secretion in response to GIP in islets in diet-induced obesity. Altered selective splicing in response to metabolic changes of the insulin receptor in β-cells was also reported (10), and hyperglycemia not only decreased total insulin receptor expression but also altered the relative expression ratio of the two insulin receptor isoforms in human islets, resulting in attenuation of insulin signal transduction. Although the mechanism of mRNA selective splicing of GIPR is unclear, insulin is reported (4) to influence the activity of the mRNA slicing regulator ASF/SF2, a serine/arginine-rich protein (SR protein). Further study is necessary to clarify the mechanism of GIPR mRNA selective splicing in response to metabolic changes.

In conclusion, we have identified a splice variant GIPR in mouse islets that has a dominant negative effect against the wild-type receptor by interacting in translocation of wild-type GIPR from the ER to the cell surface. Thus, reduced expression of truncated GIPR due to selective splicing and subsequent GIPR hypersensitivity to GIP may be involved in increased insulin secretion in response to GIP in metabolic states such as obesity.

ACKNOWLEDGMENTS

We thank K. Yamada and Dr. M. Sasaki for technical help.

GRANTS

This study was supported by Scientific Research Grants from the Ministry of Education, Culture, Sports, Science, and Technology (Japan); Health and Labor Sciences Research Grants for Comprehensive Research on Aging and Health from the Ministry of Health, Labor, and Welfare (Japan); and the 21st Century Center of Excellence Program (Japan).

REFERENCES

1. **Andersson H, D'Antona AM, Kendall DA, Von Heijne G, Chin CN.** Membrane assembly of the cannabinoid receptor 1: impact of a long N-terminal tail. *Mol Phamacol* 64: 570–577, 2003.
2. **Boylan MO, Jepeal LI, Wolfe MM.** Structure of the rat glucose-dependent insulinotropic polypeptide receptor gene. *Peptides* 20: 219–228, 1999.
3. **Creuzfeldt W, Ebert R, Willms B, Frerichs H, Brown JC.** Gastric inhibitory polypeptide (GIP) and insulin in obesity: increased response to stimulation and defective feedback control of serum levels. *Diabetologia* 14: 15–24, 1983.
4. **Diamond RH, Du K, Lee VM, Mohn KL, Haber BA, Tewari DS, Taub R.** Novel delayed-early and highly insulin-induced growth response genes. Identification of HRS, a potential regulator of alternative pre-mRNA splicing. *J Biol Chem* 268: 15185–15192, 1993.
5. **Duvernay MT, Filipeanu CM, Wu G.** The regulatory mechanisms of export trafficking of G protein-coupled receptors. *Cell Signal* 17: 1457–1465, 2005.
6. **Flatt PR, Bailey CJ, Kwasowski P, Swanston-Flatt SK, Marks V.** Abnormalities of GIP in spontaneous syndromes of obesity and diabetes in mice. *Diabetes* 32: 433–435, 1983.
7. **Gremlich S, Porret A, Hani EH, Cherif D, Vionnet N, Froguel P, Thorens B.** Cloning, functional expression, and chromosomal localization of the human pancreatic islet glucose-dependent insulinotropic polypeptide receptor. *Diabetes* 44: 1202–1208, 1995.
8. **Hague C, Uberti MA, Chen Z, Hall RA, Minneman KP.** Cell surface expression of α_{1D}-adrenergic receptors is controlled by heterodimerization with α_{1B}-adrenergic receptors. *J Biol Chem* 279: 15541–15549, 2004.
9. **Holst JJ, Gromada J, Nauck MA.** The pathogenesis of NIDDM involves a defective expression of the GIP receptor. *Diabetologia* 40: 984–986, 1997.
10. **Hribal ML, Perego L, Lovari S, Andreozzi F, Menghini R, Perego C, Finzi G, Usellini L, Placidi C, Capella C, Guzzi V, Lauro D, Bertuzzi F, Davalli A, Pozza G, Pontiroli A, Federici M, Lauro R, Brunetti A, Folli F, Sesti G.** Chronic hyperglycemia impairs insulin secretion by affecting insulin receptor expression, splicing, and signaling in RIN beta cell line and human islets of Langerhans. *FASEB J* 17: 1340–1342, 2003.
11. **Ishihara T, Nakamura S, Kaziro Y, Takahashi T, Takahashi K, Nagata S.** Molecular cloning and expression of a cDNA encoding the secretin receptor. *EMBO J* 7: 1635–1641, 1991.
12. **Jones KA, Tamm JA, Craig DA, Durkin MM, Dai M, Yao WJ, Johnson M, Gunwaldsen C, Huang LY, Tang C, Shen Q, Salon JA, Morse K, Laz T, Smith KE, Nagarathnam D, Noble SA, Branchek TA, Gerald C.** GABA(B) receptors function as a heteromeric assembly of the subunits GABA(B)R1 and GABA(B)R2. *Nature* 396: 674–679, 1998.
13. **Jordan BA, Trapaidze N, Gomes I, Nivarthi R, Devi LA.** Oligomerization of opioid receptors with β_2-adrenergic receptors: a role in trafficking and mitogen-activated protein kinase activation. *Proc Natl Acad Sci USA* 98: 343–348, 2001.
14. **Kahn BB, Flier JS.** Obesity and insulin resistance. *J Clin Invest* 106: 473–481, 2000.
15. **Kubota A, Yamada Y, Hayami T, Yasuda K, Someya Y, Ihara Y, Kagimoto S, Watanabe R, Taminato T, Tsuda K, Seino Y.** Identification of two missense mutations in the GIP receptor gene: a functional study and association analysis with NIDDM: no evidence of association with Japanese NIDDM subjects. *Diabetes* 45: 1701–1705, 1996.
16. **Lemieux I, Pascot A, Couillard C, Lamarche B, Tchernof A, Alméras N, Bergeron J, Gaudet D, Tremblay G, Prud'homme D, Nadeau A, Després JP.** Hypertriglyceridemic waist: A marker of the atherogenic metabolic triad (hyperinsulinemia; hyperapolipoprotein B; small, dense LDL) in men? *Circulation* 102: 179–184, 2000.
17. **Lynn FC, Pamir N, Ng EH, McIntosh CH, Kieffer TJ, Pederson RA.** Defective glucose-dependent insulinotropic polypeptide receptor expression in diabetic fatty Zucker rats. *Diabetes* 50: 1004–1011, 2001.
18. **Lynn FC, Thompson SA, Pospisilik JA, Ehses JA, Hinke SA, Pamir N, McIntosh CH, Pederson RA.** A novel pathway for regulation of glucose-dependent insulinotropic polypeptide (GIP) receptor expression in beta cells. *FASEB J* 17: 91–93, 2003.
19. **Margeta-Mitrovic M, Jan YN, Jan LY.** Function of GB1 and GB2 subunits in G protein coupling of GABA(B) receptors. *Proc Natl Acad Sci USA* 98: 14649–14654, 2001.
20. **Miyawaki K, Yamada Y, Ban N, Ihara Y, Tsukiyama K, Zhou H, Fujimoto S, Oku A, Tsuda K, Toyokuni S, Hiai H, Mizunoya W, Fushiki T, Holst JJ, Makino M, Tashita A, Kobara Y, Tsubamoto Y, Jinnouchi T, Jomori T, Seino Y.** Inhibition of gastric inhibitory polypeptide signaling prevents obesity. *Nat Med* 8: 738–742, 2002.
21. **Miyawaki K, Yamada Y, Yano H, Niwa H, Ban N, Ihara Y, Kubota A, Fujimoto S, Kajikawa M, Kuroe A, Tsuda K, Hashimoto H, Yamashita T, Jomori T, Tashiro F, Miyazaki J, Seino Y.** Glucose intolerance caused by a defect in the entero-insular axis: a study in gastric inhibitory polypeptide receptor knockout mice. *Proc Natl Acad Sci USA* 96: 14843–14847, 1999.
22. **Mukai E, Ishida H, Kato S, Tsura Y, Fujimoto S, Takahashi A, Horie M, Tsuda K, Seino Y.** Metabolic inhibition impairs ATP-sensitive K^+ channel block by sulfonylurea in pancreatic β-cells. *Am J Physiol Endocrinol Metab* 274: E38–E44, 1998.
23. **Nakamura Y, Suzuki H, Sakaguchi M, Mihara K.** Targeting and assembly of mitochondrial translocase of outer membrane 22 (TOM22) into the TOM complex. *J Biol Chem* 279: 21223–21232, 2004.
24. **Pederson RA.** GIP. *Gut Peptides*, edited by Walsh J and Dockray G. New York: Raven, 1993, p. 217–259.
25. **Reaven GM.** Role of insulin resistance in human disease. *Diabetes* 37: 1066–1084, 1988.
26. **Salahpour A, Angers S, Mercier JF, Lagace M, Marullo S, Bouvier M.** Homodimerization of the β2-adrenergic receptor as a prerequisite for cell surface targeting. *J Biol Chem* 279: 33390–33397, 2004.
27. **Service FJ, Rizza RA, Westland RE, Hall LD, Gerich JE, Go VL.** Gastric inhibitory polypeptide in obesity and diabetes mellitus. *J Clin Endocrinol Metab* 58: 1133–1140, 1984.

Downloaded from ajpendo.physiology.org on February 28, 2008

28. **Stock S, Leichner P, Wong AC, Ghatei MA, Kieffer TJ, Bloom SR, Chanoine JP.** Ghrelin, peptide YY, glucose-dependent insulinotropic polypeptide, and hunger responses to a mixed meal in anorexic, obese, and control female adolescents. *J Clin Endocrinol Metab* 90: 2161–2168, 2005.
29. **Sutton R, Peters M, McShane P, Gray DW, Morris PJ.** Isolation of rat pancreatic islets by ductal injection of collagenase. *Transplantation* 42: 689–691, 1986.
30. **Tsukiyama K, Yamada Y, Yamada C, Harada N, Kawasaki Y, Ogura M, Bessho K, Li M, Amizuka N, Sato M, Udagawa N, Takahashi N, Tanaka K, Oiso Y, Seino Y.** Gastric inhibitory polypeptide as an endogenous factor promoting new bone formation following food ingestion. *Mol Endocrinol* 20: 1644–1651, 2006.
31. **Usdin TB, Mezey E, Button DC, Brownstein MJ, Bonner TI.** Gastric inhibitory polypeptide receptor, a member of the secretin-vasoactive intestinal peptide receptor family, is widely distributed in peripheral organs and the brain. *Endocrinology* 133: 2861–2870, 1993.
32. **Volz A, Göke R, Lankat-Buttgereit B, Fehmann HC, Bode HP, Goke B.** Molecular cloning, functional expression, and signal transduction of the GIP-receptor cloned from a human insulinoma. *FEBS Lett* 373: 23–29, 1995.
33. **Yamada Y, Hayami T, Nakamura K, Kaisaki PJ, Someya Y, Wang CZ, Seino S, Seino Y.** Human gastric inhibitory polypeptide receptor: cloning of the gene (GIPR) and cDNA. *Genomics* 29: 773–776, 1995.

Downloaded from ajpendo.physiology.org on February 28, 2008

Available online at www.sciencedirect.com
ScienceDirect
Biochemical and Biophysical Research Communications 366 (2008) 174–179
BBRC
www.elsevier.com/locate/ybbrc

Localization of mouse mitochondrial SIRT proteins: Shift of SIRT3 to nucleus by co-expression with SIRT5

Yasuhiko Nakamura, Masahito Ogura, Daisuke Tanaka, Nobuya Inagaki *

Department of Diabetes and Clinical Nutrition, Graduate School of Medicine, Kyoto University, 54 Kawahara-cho, Shogoin, Sakyo-ku, Kyoto 606-8507, Japan

Received 13 November 2007
Available online 3 December 2007

Abstract

Yeast silent information regulator 2 (SIR2) is involved in extension of yeast longevity by calorie restriction, and SIRT3, SIRT4, and SIRT5 are mammalian homologs of SIR2 localized in mitochondria. We have investigated the localization of these three SIRT proteins of mouse. SIRT3, SIRT4, and SIRT5 proteins were localized in different compartments of the mitochondria. When SIRT3 and SIRT5 were co-expressed in the cell, localization of SIRT3 protein changed from mitochondria to nucleus. These results suggest that the SIRT3, SIRT4, and SIRT5 proteins exert distinct functions in mitochondria. In addition, the SIRT3 protein might function in nucleus.
© 2007 Elsevier Inc. All rights reserved.

Keywords: SIRT3; SIRT4; SIRT5; Intramitochondrial localization; Localization shift

Silent information regulator 2 (SIR2) is the enzyme that catalyzes NAD^+-dependent protein deacetylation and produces nicotinamide and *O*-acetyl-ADP-ribose [1,2], and is localized in nucleus [3]. In yeast, lifespan is prolonged in low glucose condition [4,5], but such lifespan extension is abolished by SIR2 gene disruption [6], suggesting that SIR2 plays an important role in determining yeast longevity. In mammals, there are seven SIR2 homologs, SIRT1–7 [7]. However, it remains unclear whether SIRTs mediate lifespan extension by calorie restriction.

Human SIRT3, SIRT4, and SIRT5 proteins are known to be localized in mitochondria [7,8]. Mouse SIRT4 was previously shown *in vivo* to ADP-ribosylate glutamate dehydrogenase and down-regulate its activity in pancreatic islets, inhibiting amino acid-stimulated insulin secretion [9]. On the other hand, recent studies have demonstrated that human SIRT3 deacetylates acetyl-CoA synthetase 2 in mitochondrial matrix *in vitro* [10,11]. Human SIRT5 has been shown to have weak deacetylase activity *in vitro* [12]. However, the function of SIRT3 and SIRT5 *in vivo* is still unknown.

Although human SIRT4 and SIRT5 proteins have been reported to localize in mitochondria, precise localization of these proteins is unknown. Regarding SIRT3, localization of SIRT3 protein has been reported to differ in mouse and human, in mitochondrial inner membrane in mouse [13] and in mitochondrial matrix in human [14]. Furthermore, there has been no report on the interaction of the three SIRT proteins known to be localized in mitochondria.

In the present study, we determined localization of mouse SIRT3, SIRT4, and SIRT5 proteins in COS7 cells in different compartments of mitochondria: inner membrane, matrix, and intermembrane space. In addition, we demonstrate that localization of SIRT3

Abbreviations: SIR2, silent information regulator 2; MTS, mitochondrial targeting signal; NLS, nuclear localization signal; GAPDH, glyceraldehyde 3-phosphate dehydrogenase; PNS, post-nuclear supernatant; PHB, prohibitin; ER, estrogen receptor.

* Corresponding author. Fax: +81 75 771 6601.
E-mail address: inagaki@metab.kuhp.kyoto-u.ac.jp (N. Inagaki).

0006-291X/$ - see front matter © 2007 Elsevier Inc. All rights reserved.
doi:10.1016/j.bbrc.2007.11.122

protein in COS7 cells changes from mitochondria to nucleus when co-expressed with SIRT5. We also address the regulatory mechanism of SIRT3 localization by a mutagenesis study of the putative mitochondrial targeting signal (MTS) and nuclear localization signal (NLS).

Materials and methods

Antibodies. The antibodies used for confocal microscopic analysis and Western blot analysis included anti-myc (Santa Cruz Biotechnology), anti-FLAG (Sigma), anti-hsp60 (BD Biosciences), anti-calnexin (Stressgen), anti-glyceraldehyde 3-phosphate dehydrogenase (GAPDH) (Santa Cruz Biotechnology), anti-cytochrome *c* (Cell Signaling), and anti-laminA/C (Cell Signaling).

Plasmid construction. The expression vector for SIRT3-myc, SIRT4-myc, SIRT4-FLAG, and SIRT5-FLAG was constructed as follows. The coding region of SIRT cDNAs was cloned by PCR using mouse liver cDNA. The PCR fragments were subcloned into the pcDNA3.1/myc-His A expression vector (Invitrogen) or the pFLAG-CMV-5a expression vector (Sigma). SIRT3nu and SIRT3mt mutants were constructed by overlap extension PCR method [15] using pcDNA3.1/myc-His-SIRT3 plasmid as the template.

Cell culture and transfection. COS7 cells were maintained in Dulbecco's modified Eagle's medium (Sigma) supplemented with 10% fetal bovine serum (Gibco) in an atmosphere of 5% CO_2 at 37 °C. DNA transfection was performed according to the manufacturer's instructions using FuGene6 Transfection Reagent (Roche). One microgram of plasmid DNA was transfected to COS7 cells in a 3.5-cm dish.

Confocal microscopy. Fluorescence microscopic analysis was performed as described previously [16]. Briefly, COS7 cells transfected with SIRT expression plasmids were fixed and labeled with anti-myc monoclonal IgG and Alexa488-conjugated anti-mouse IgG (Molecular Probes) or anti-FLAG polyclonal IgG and Cy3-conjugated anti-rabbit IgG (Sigma). Fluorescent images were taken and analyzed using a confocal laser microscope (LSM510 META; Carl Zeiss).

Fractionation of post-nuclear supernatant. Fractionation of post-nuclear supernatant was performed as described previously [17]. Twenty micrograms of plasmid DNA was transfected to COS7 cells in a 10-cm dish. The transfected cells were harvested and disrupted in isotonic buffer (PBS containing 0.2 M mannitol, 0.07 M sucrose, and 1 mM EDTA) containing protease inhibitors (Complete, EDTA Free; Roche) with potter homogenizer, followed by centrifuged at 800*g* at 4 °C for 10 min to obtain post-nuclear supernatant (PNS). PNS was centrifuged at 10,000*g* at 4 °C for 10 min to obtain the mitochondria-enriched precipitate fraction. The supernatant was centrifuged at 100,000*g* at 4 °C for 30 min to separate the microsome-enriched precipitate and supernatant fractions. The subcellular fractions were separated by SDS–PAGE and then analyzed by Western blotting.

Alkaline treatment of mitochondria. Mitochondria were prepared from the COS7 cells expressing each SIRT protein, and treated with 100 mM Na_2CO_3 in 10 times volume of mitochondria suspension for 1 h on ice. The reaction mixtures were centrifuged at 100,000*g* at 4 °C for 30 min to separate the precipitate and supernatant fractions. The fractions were subjected to SDS–PAGE followed by Western blot analysis.

Submitochondrial fractionation. The mitochondria were treated with either H_2O or 2% TX-100 in 10 times volume of mitochondria suspension on ice for 1 h, and then treated with 50 μg/ml trypsin on ice for 1 h. The reaction mixtures were separated by SDS–PAGE and then analyzed by Western blotting.

Subcellular fractionation using digitonin. The transfected COS7 cells were harvested and lysed with PBS containing 2% digitonin. The cell lysate was centrifuged at 800*g* at 4 °C for 10 min to obtain nucleus-enriched insoluble and soluble fractions. The fractions were separated by SDS–PAGE and then analyzed by Western blotting.

Results and discussion

Distinct localizations of SIRT3, SIRT4, and SIRT5 in mitochondria

To determine the intracellular localization of mouse SIRT3, SIRT4, and SIRT5 proteins, expression plasmid encoding each of these SIRT proteins fused with myc tag or FLAG tag at the C terminus was transfected into COS7 cells. The SIRT proteins were stained with anti-myc antibody or anti-FLAG antibody and its intracellular localization was examined using confocal microscopy (Fig. 1A). All three images of SIRT3, SIRT4, and SIRT5 proteins merged well with that of MitoTracker Red, a marker of mitochondria, indicating that all of these SIRT proteins are localized in mitochondria. Cell fractionation was then performed using cells transfected with the SIRT expression plasmids. PNS of the cells was centrifuged and fractionated into the mitochondria-enriched low-speed precipitate (P1), the microsome-enriched high-speed precipitate (P2), and the supernatant (S) fractions (Fig. 1B). All of the three SIRT proteins were found in the P1 fraction as was hsp60 protein, a marker of mitochondria, affirming their localization in mitochondria.

To clarify localization of the three SIRT proteins in mitochondria, mitochondrial fraction prepared from COS7 cells expressing each of the SIRT proteins was treated with Na_2CO_3 and centrifuged. SIRT3 protein was detected in the precipitate fraction, while SIRT4 and SIRT5 proteins were detected in the supernatant fraction, indicating that SIRT3 protein is integrated into either mitochondrial outer or inner membrane and that SIRT4 and SIRT5 are soluble and not membrane proteins (Fig. 1C). After treating the mitochondrial fractions with either H_2O or TX-100, the fractions were treated with trypsin. When mitochondria are treated with H_2O, the mitoplast can be obtained. SIRT3 and SIRT5 proteins were digested with trypsin in both H_2O- and TX-100-treated mitochondria but were not digested in untreated mitochondria (Fig. 1D), indicating that these proteins are localized either in intermembrane space or in inner membrane. In contrast, SIRT4 was digested only in the TX-100-treated mitochondria. Taken together, these results indicate that SIRT3, SIRT4, and SIRT5 proteins are localized in inner membrane, matrix, and intermembrane space, respectively, in mitochondria. In human, SIRT3 protein was reported to localize in mitochondrial matrix [14]. Since mouse SIRT3 protein lacks a region corresponding to the N-terminal 142-amino acid residues of human SIRT3 protein, the region could be critical in determining localization in mitochondria. In addition, the function of SIRT3 might differ in humans and mice.

SIRT3 is localized in nucleus when co-expressed with SIRT5

We then examined localization of these three mitochondrial SIRT proteins when two of them were co-expressed in

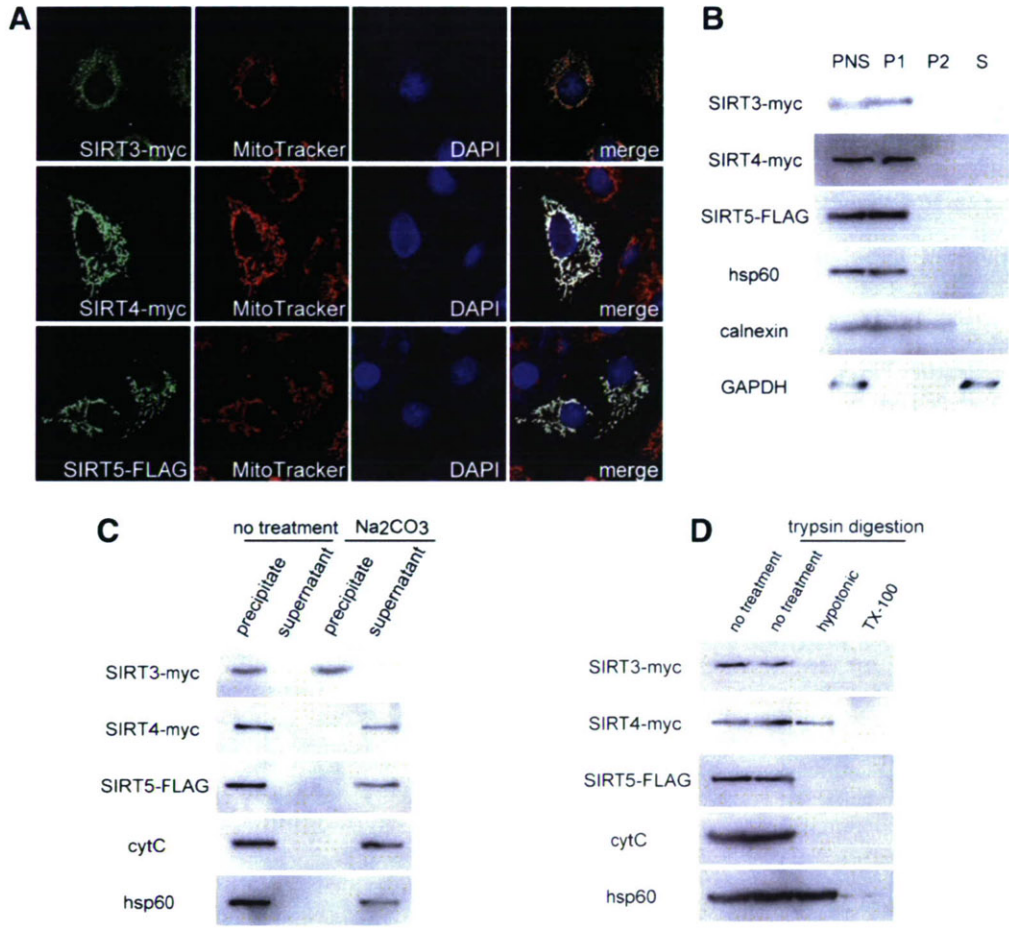

Fig. 1. Localization of SIRT3, SIRT4, and SIRT5 in mitochondria. (A) Confocal microscopy. SIRT3-myc (upper panels), SIRT4-myc (middle panels), and SIRT5-FLAG (lower panels) were expressed in COS7 cells and immunostained with anti-myc antibody or anti-FLAG antibody. Mitochondria and nuclei were stained by MitoTracker Red and DAPI, respectively, and fluorescent images were obtained using a confocal microscope. (B) Fractionation of post-nuclear supernatant. SIRT3-myc, SIRT4-myc, and SIRT5-FLAG proteins each was expressed in COS7 cells, and the obtained PNS was fractionated into mitochondria-enriched precipitate (P1), microsome-enriched precipitate (P2), and supernatant (S) fractions. The three fractions were separated by SDS–PAGE and then analyzed by Western blotting using anti-myc antibody for SIRT3-myc and SIRT4-myc or anti-FLAG antibody for SIRT5-FLAG. Hsp60, calnexin, and GAPDH were used as endogenous markers for mitochondria, microsome, and cytosol, respectively. (C) Alkaline treatment of mitochondria. Mitochondria prepared from the COS7 cells expressing each of the SIRT3-myc, SIRT4-myc, and SIRT5-FLAG proteins were treated with Na_2CO_3. The reaction mixture was centrifuged to separate the precipitate and supernatant fractions, containing membrane-integrated proteins and soluble proteins, respectively. The two fractions were analyzed by Western blotting. Cytochrome *c* (cyt*c*) and hsp60 were used as endogenous protein markers for mitochondrial soluble protein. (D) Submitochondrial fractionation. The mitochondria from COS7 cells expressing one of three SIRT proteins were treated with either H_2O (hypotonic) or TX-100, and then treated with trypsin. The reaction mixtures were analyzed by Western blotting. Cytochrome *c* and hsp60 were used as endogenous markers for mitochondrial intermembrane space protein and matrix protein, respectively.

COS7 cells (Fig. 2A). When SIRT3 and SIRT5 proteins were co-expressed, the localization of SIRT3 protein but not SIRT5 protein changed from mitochondria to nucleus (upper panels). However, SIRT proteins remained in mitochondria with the other combinations of co-expression (SIRT3 and SIRT4, middle panels, and SIRT4 and SIRT5, lower panels). To confirm the localization shift of SIRT3 protein by co-expression with SIRT5, we performed fractionation of PNS (Fig. 2B). SIRT5 protein appears in P1 fraction, indicating its localization in mitochondria. In contrast, SIRT3 protein is not found in PNS but appears in whole cell lysate, indicating that SIRT3 is localized in nucleus. These results are consistent with confocal microscopic study. In addition, we performed another cell fractionation to separate nucleus and the remaining portion of the cell using digitonin (Fig. 2C). The nuclear proteins lamin A/C appeared in insoluble (INS) fraction and the mitochondrial protein hsp60 occurred in both insoluble and soluble (SOL) fractions to a similar extent. SIRT3 protein also was detected in both insoluble and soluble fractions to a similar extent when expressed alone. However, the majority of SIRT3 protein was detected in the insoluble fraction when co-expressed with SIRT5, further confirming the localization shift of SIRT3 protein from mitochondria to nucleus. Taken together, we clearly show here for the first time that the intracellular localization of SIRT3 protein changes from mitochondria to nucleus in the presence of SIRT5, suggesting that SIRT3 plays a role as a regulator of nuclear proteins through its deacetylase or other, unknown activity.

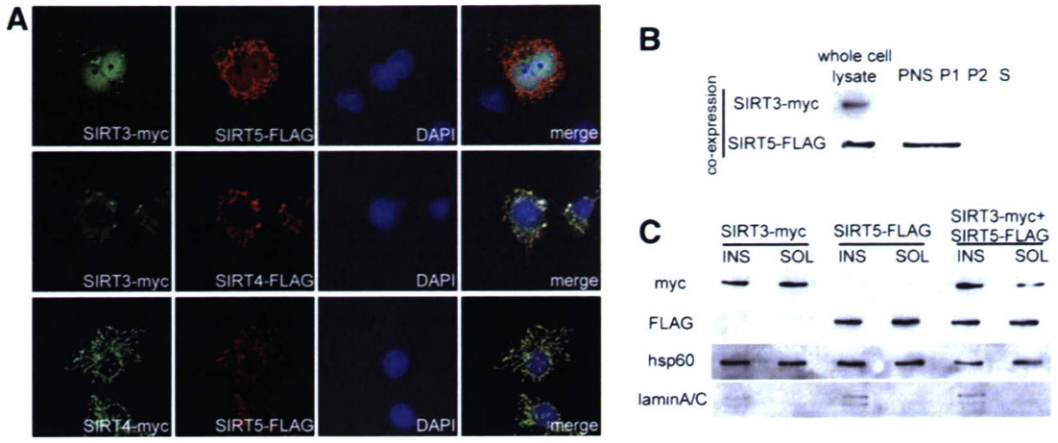

Fig. 2. Localization of SIRT3 when co-expressed with SIRT5. (A) Confocal microscopic analysis of COS7 cells expressing two of the three mitochondrial SIRT proteins. SIRT3-myc and SIRT5-FLAG (upper panels), SIRT3-myc and SIRT4-FLAG (middle panels), and SIRT4-myc and SIRT5-FLAG (lower panels) were co-expressed in COS7 cells, and immunostained using antibodies against myc tag and FLAG tag. Nuclei were stained by DAPI. (B) Subcellular fractionation of PNS. PNS of COS7 cells co-expressing SIRT3-myc and SIRT5-FLAG was fractionated into mitochondria-enriched precipitate (P1), microsome-enriched precipitate (P2), and supernatant (S) fractions, and these fractions along with whole cell lysate were analyzed by Western blotting. (C) Subcellular fractionation using digitonin. COS7 cells expressing either SIRT3-myc (left) or SIRT5-FLAG (middle) or both (right) were solubilized by digitonin, and the obtained lysate was centrifuged and fractionated into nuclear-enriched insoluble (INS), and soluble (SOL) fractions. Hsp60 and laminA/C were used as endogenous markers for mitochondria protein and nucleus protein, respectively.

Disruption of putative mitochondrial targeting signal of SIRT3

Because the segment containing amino acid residues 66–88 potentially forms a basic amphiphilic α-helical structure, it could serve as a MTS. To examine the role of this segment, SIRT3 mutant SIRT3mt, in which the four amino acid residues 72–75 were replaced by four alanine residues, was constructed (Fig. 3A). When SIRT3mt alone was expressed in COS7 cells, SIRT3mt protein was not detected in mitochondria but was widely distributed in the cell in confocal microscopic analysis (Fig. 3B, upper panels). In addition, when SIRT3mt and SIRT5 were co-expressed, the distribution of SIRT3mt protein was not changed compared to that expressed alone (Fig. 3B, lower panels). In fractionation of PNS, SIRT3mt protein was fractionated into S fraction both when SIRT3mt was expressed alone and when SIRT3mt and SIRT5 were co-expressed. SIRT5 protein was localized in mitochondria when SIRT3mt and SIRT5 were co-expressed (Fig. 3C). These results indicate that the MTS is necessary not only for targeting SIRT3 to mitochondria in the absence of SIRT5 but also for targeting SIRT3 to nucleus in the presence of SIRT5.

Disruption of putative nuclear localization signal of SIRT3

We found that the sequence containing amino acid residues 213–219 of the SIRT3 protein closely resembles the

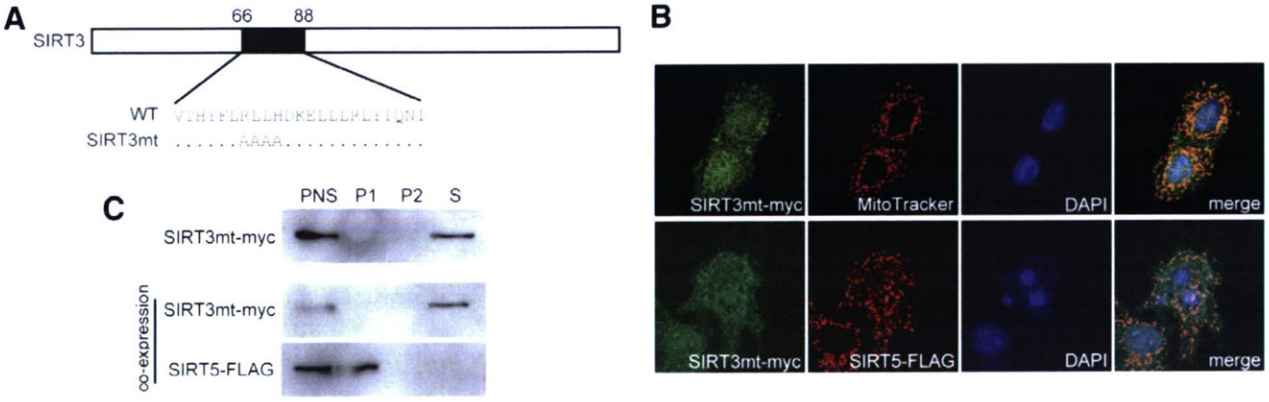

Fig. 3. Effect of disruption of putative mitochondrial targeting signal of SIRT3. (A) Alanine replacement of putative MTS of SIRT3. Four residues of the putative MTS of SIRT3 (amino acid residues 72–75) were replaced with four alanine residues. In the SIRT3mt sequence, amino acid residues identical with wild-type SIRT3 protein are indicated with dots. (B) Confocal microscopy. Immunofluorescent images of COS7 cells expressing SIRT3mt-myc alone (upper panels) or both SIRT3mt-myc and SIRT5-FLAG (lower panels) are shown. Mitochondria and nuclei were stained by MitoTracker Red and DAPI, respectively. (C) Subcellular fractionation of PNS. PNSs of COS7 cells expressing SIRT3mt-myc alone (an upper panel) or co-expressing SIRT3mt-myc and SIRT5-FLAG (middle and lower panels) were centrifuged and fractionated into mitochondria-enriched precipitate (P1), microsome-enriched precipitate (P2), and supernatant (S) fractions. The fractions were analyzed by Western blotting.

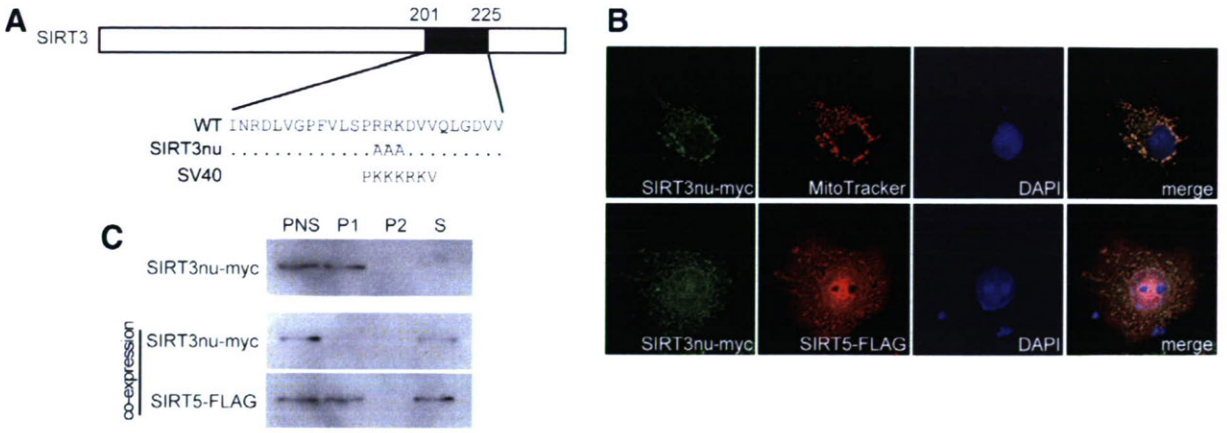

Fig. 4. Effect of disruption of putative nuclear localization signal of SIRT3. (A) Comparison of the amino acid sequences of putative NLS of SIRT3, SIRT3nu, and SV40 large T antigen. Three basic amino acid residues of the putative NLS of SIRT3 (amino acid residues 214–216) were replaced with three alanine residues. In the SIRT3nu sequence, amino acid residues identical with wild-type SIRT3 protein are indicated with dots. The classical NLS of SV40 large T antigen also is shown (SV40). (B) Confocal microscopy. Immunofluorescent images of COS7 cells expressing SIRT3nu-myc alone (upper panels) or both SIRT3nu-myc and SIRT5-FLAG (lower panels) are shown. Mitochondria and nuclei were stained by MitoTracker Red and DAPI, respectively. (C) Subcellular fractionation of PNS. PNSs of the COS7 cells expressing SIRT3nu-myc alone (an upper panel) or co-expressing SIRT3nu-myc and SIRT5-FLAG (middle and lower panels) were fractionated into mitochondria-enriched precipitate (P1), microsome-enriched precipitate (P2), and supernatant (S) fractions. The fractions were analyzed by Western blotting.

classical NLS of the SV40 T antigen (Fig. 4A). To examine whether this sequence functions as a NLS, the mutant SIRT3 protein SIRT3nu, in which the three basic amino acid residues (214–216) in the putative NLS of SIRT3 were replaced by three alanine residues (Fig. 4A), was constructed. When SIRT3nu alone was expressed in COS7 cells, it was localized in mitochondria (Fig. 4B, upper panels). In the cells co-expressing SIRT3nu and SIRT5, a shift of SIRT3nu protein to the nucleus was not observed, and SIRT3nu protein and a part of SIRT5 protein were scattered widely in the cell in confocal microscopic analysis (Fig. 4B, lower panels). In fractionation of PNS, all of the SIRT3nu protein and nearly half of the SIRT5 protein were shifted from P1 fraction to S fraction by co-expression (Figs. 1B and 4C). These results suggest that the segment containing amino acid residues 213–219 of SIRT3 plays an important role in the localization shift of SIRT3 protein to nucleus when co-expressed with SIRT5. Furthermore, SIRT5 may well hamper SIRT3nu localization in mitochondria through interaction with SIRT3nu. However, further study is required to elucidate the mechanism of the localization shift of SIRT3 protein.

Interestingly, recent study has reported that human prohibitin 2 (PHB2), known as a repressor of estrogen receptor (ER) activity, is localized in the mitochondrial inner membrane, and translocates to the nucleus in the presence of ER and estradiol [18]. Although the mechanism of regulation of the expression level of SIRT5 remains unknown, SIRT3 might play a role in communication between nucleus and mitochondria in a SIRT5-dependent manner.

The function of mitochondrial SIRT proteins is still not well known. In the present study, we determined the exact localization of mouse SIRT3, SIRT4, and SIRT5 proteins in mitochondria. In addition, we demonstrated that SIRT3 can be present in nucleus in the presence of SIRT5. It has been reported that SIRT3 deacetylates proteins that are not localized in mitochondria *in vitro* such as histone-4 peptide and tubulin [14]. Thus, if SIRT3 is present in nucleus *in vivo*, SIRT3 protein might well deacetylate nuclear proteins. These results provide useful information for the investigation of the function of these proteins.

Acknowledgments

This work was supported by Scientific Research Grants and a Grant-in-Aid for Creative Scientific Research 15GS0301 from the Ministry of Education, Culture, Sports, Science, and Technology of Japan.

References

[1] J.C. Tanny, G.J. Dowd, J. Huang, H. Hilz, D. Moazed, An enzymatic activity in the yeast Sir2 protein that is essential for gene silencing, Cell 99 (1999) 735–745.
[2] S. Imai, C.M. Armstrong, M. Kaeberlein, L. Guarente, Transcriptional silencing and longevity protein Sir2 is an NAD-dependent histone deacetylase, Nature 403 (2000) 795–800.
[3] M. Gotta, S. Strahl-Bolsinger, H. Renauld, T. Laroche, B.K. Kennedy, M. Grunstein, S.M. Gasser, Localization of Sir2p: the nucleolus as a compartment for silent information regulators, EMBO J. 16 (1997) 3243–3255.
[4] I. Muller, M. Zimmermann, D. Becker, M. Flomer, Calendar life span versus budding life span of *Saccharomyces cerevisiae*, Mech. Aging Dev. 12 (1980) 47–52.
[5] S.J. Lin, M. Kaeberlein, A.A. Andalis, L.A. Sturtz, P.A. Defossez, V.C. Culotta, G.R. Fink, L. Guarente, Calorie restriction extends *Saccharomyces cerevisiae* lifespan by increasing respiration, Nature 418 (2002) 344–348.
[6] S.J. Lin, P.A. Defossez, L. Guarente, Requirement of NAD and SIR2 for life-span extension by calorie restriction in *Saccharomyces cerevisiae*, Science 289 (2000) 2126–2128.

[7] E. Michishita, J.Y. Park, J.M. Burneskis, J.C. Barrett, I. Horikawa, Evolutionarily conserved and nonconserved cellular localizations and functions of human SIRT proteins, Mol. Biol. Cell 16 (2005) 4623–4635.
[8] P. Onyango, I. Celic, J.M. McCaffery, J.D. Boeke, A.P. Feinberg, SIRT3, a human SIR2 homologue, is an NAD-dependent deacetylase localized to mitochondria, Proc. Natl. Acad. Sci. USA 99 (2002) 13653–13658.
[9] M.C. Haigis, R. Mostoslavsky, K.M. Haigis, K. Fahie, D.C. Christodoulou, A.J. Murphy, D.M. Valenzuela, G.D. Yancopoulos, M. Karow, G. Blander, C. Wolberger, T.A. Prolla, R. Weindruch, F.W. Alt, L. Guarente, SIRT4 inhibits glutamate dehydrogenase and opposes the effects of calorie restriction in pancreatic β cells, Cell 126 (2006) 941–954.
[10] B. Schwer, J. Bunkenborg, R.O. Verdin, J.S. Andersen, E. Verdin, Reversible lysine acetylation controls the activity of the mitochondrial enzyme acetyl-CoA synthetase 2, Proc. Natl. Acad. Sci. USA 103 (2006) 10224–10229.
[11] W.C. Hallows, S. Lee, J.M. Denu, Sirtuins deacetylate and activate mammalian acetyl-CoA synthetases, Proc. Natl. Acad. Sci. USA 103 (2006) 10230–10235.
[12] B.J. North, B.L. Marshall, M.T. Borra, J.M. Denu, E. Verdin, The human Sir2 ortholog, SIRT2, is an NAD^+-dependent tubulin deacetylase, Mol. Cell 11 (2003) 437–444.
[13] T. Shi, F. Wang, E. Stieren, Q. Tong, SIRT3, a mitochondrial sirtuin deacetylase, regulates mitochondrial function and thermogenesis in brown adipocytes, J. Biol. Chem. 280 (2005) 13560–13567.
[14] B. Schwer, B.J. North, R.A. Frye, M. Ott, E. Verdin, The human silent information regulator (Sir)2 homologue hSIRT3 is a mitochondrial nicotinamide adenine dinucleotide-dependent deacetylase, J. Cell Biol. 158 (2002) 647–657.
[15] S.N. Ho, H.D. Hunt, R.M. Horton, J.K. Pullen, L.R. Pease, Site-directed mutagenesis by overlap extension using the polymerase chain reaction, Gene 77 (1989) 51–59.
[16] Y. Matsumura, N. Ban, K. Ueda, N. Inagaki, Characterization and classification of ATP-binding cassette transporter ABCA3 mutants in fatal surfactant deficiency, J. Biol. Chem. 281 (2006) 34503–34514.
[17] Y. Nakamura, H. Suzuki, M. Sakaguchi, K. Mihara, Targeting and assembly of rat mitochondrial translocase of outer membrane 22 (TOM22) into the TOM complex, J. Biol. Chem. 279 (2004) 21223–21232.
[18] K. Kasashima, E. Ohta, Y. Kagawa, H. Endo, Mitochondrial functions and estrogen receptor-dependent nuclear translocation of pleiotropic human prohibitin 2, J. Biol. Chem. 281 (2006) 36401–36410.

0013-7227/08/$15.00/0
Printed in U.S.A.

Endocrinology 149(2):574–579
Copyright © 2008 by The Endocrine Society
doi: 10.1210/en.2007-1292

The Murine Glucagon-Like Peptide-1 Receptor Is Essential for Control of Bone Resorption

Chizumi Yamada, Yuichiro Yamada, Katsushi Tsukiyama, Kotaro Yamada, Nobuyuki Udagawa, Naoyuki Takahashi, Kiyoshi Tanaka, Daniel J. Drucker, Yutaka Seino, and Nobuya Inagaki

Department of Diabetes and Clinical Nutrition (C.Y., Y.Y., K.T., K.Y., Y.S., N.I.), Kyoto University Graduate School of Medicine, and Core Research for Evolutional Science and Technology of Japan Science and Technology Cooperation (N.I), Kyoto 606-8507, Japan; Department of Internal Medicine (Y.Y.), Division of Endocrinology, Diabetes and Geriatric Medicine, Akita University School of Medicine, Akita 010-8543, Japan; Department of Biochemistry (N.U.) and Institute for Oral Science (N.T.), Matsumoto Dental University, Nagano 399-0781, Japan; Department of Nutrition (K.T.), Kyoto Women's University, Kyoto 605-8501, Japan; The Samuel Lunenfeld Research Institute (D.J.D.), Department of Medicine, Mount Sinai Hospital and the Banting and Best Diabetes Center, University of Toronto, Toronto, Canada M5G 2C4; Kansai Electric Power Hospital (Y.S.), Osaka 553-0003, Japan

Gastrointestinal hormones including gastric inhibitory polypeptide (GIP), glucagon-like peptide (GLP)-1, and GLP-2 are secreted immediately after meal ingestion, and GIP and GLP-2 have been shown to regulate bone turnover. We hypothesize that endogenous GLP-1 may also be important for control of skeletal homeostasis. We investigated the role of GLP-1 in the regulation of bone metabolism using GLP-1 receptor knockout (Glp-1r$^{-/-}$) mice. A combination of bone density and histomorphometry, osteoclast activation studies, biochemical analysis of calcium and PTH, and RNA analysis was used to characterize bone and mineral homeostasis in Glp-1r$^{-/-}$ and Glp-1r$^{+/+}$ littermate controls. Glp-1r$^{-/-}$ mice have cortical osteopenia and bone fragility by bone densitometry as well as increased osteoclastic numbers and bone resorption activity by bone histomorphometry. Although GLP-1 had no direct effect on osteoclasts and osteoblasts, Glp-1r$^{-/-}$ mice exhibited higher levels of urinary deoxypyridinoline, a marker of bone resorption, and reduced levels of calcitonin mRNA transcripts in the thyroid. Moreover, calcitonin treatment effectively suppressed urinary levels of deoxypyridinoline in Glp-1r$^{-/-}$, mice and the GLP-1 receptor agonist exendin-4 increased calcitonin gene expression in the thyroid of wild-type mice. These findings establish an essential role for endogenous GLP-1 receptor signaling in the control of bone resorption, likely through a calcitonin-dependent pathway. (*Endocrinology* 149: 574–579, 2008)

BONE IS CONTINUOUSLY remodeled throughout life, and osteoblastic bone formation and osteoclastic bone resorption are closely coordinated by a variety of local and systemic factors to maintain constant bone mass. Bone resorption is known to be rapidly inhibited by acute nutrient ingestion, suggesting that it might be mediated by other physiological factors, the levels of which change in response to the nutritional state such as incretins. Gastrointestinal hormones including gastric inhibitory polypeptide (GIP), glucagon-like peptide (GLP)-1, and GLP-2 are secreted immediately upon meal ingestion, although the fasting level of these peptides is low. GIP and GLP-2 are known to be involved in the regulation of bone turnover (1, 2).

The effect of GIP on bone has been extensively investigated *in vitro* and *in vivo*. The GIP receptor is expressed in osteoblasts (3), and GIP increases collagen type 1 expression and alkaline phosphatase activity in osteoblast-like cells (3) and protects osteoblasts from apoptosis (2), consistent with an anabolic effect. Recently, the presence of the GIP receptor in osteoclasts has been reported, and GIP has been shown to inhibit PTH-induced bone resorption, suggesting that a role of the postprandial rise in GIP is to stop active bone resorption such as occurs during fasting (4). The physiological importance of GIP receptor signaling on bone *in vivo* has been demonstrated using GIP receptor knockout (Gipr$^{-/-}$) mice, which exhibit a low bone mass phenotype due to both decreased bone formation and increased bone resorption (2, 5); and conversely, GIP-overexpressing transgenic mice exhibit increased bone mass (6).

GLP-2 is cosecreted with GLP-1 from L cells in the small and large intestine, and acts in the intestine to stimulate mucosal growth and nutrient absorption. Acute administration of GLP-2 decreases serum and urine markers of bone resorption in postmenopausal women (1, 7, 8), whereas bone formation appears to be unaffected by treatment with exogenous GLP-2. The effect of GLP-2 on bone has been investigated predominantly in humans, and the mechanism(s) underlying the GLP-2-mediated modulation of bone turnover remain unclear.

GLP-1 is well known as an incretin, and meal-stimulated plasma levels of GLP-1 are known to be diminished in patients with impaired glucose tolerance or type 2 diabetes (9). GLP-1 also has effects independent of insulin secretion such as inhibition of glucagon secretion and gastric emptying. In

First Published Online November 26, 2007

Abbreviations: BMC, Bone mineral content; BMD, bone mineral density; BS, bone surface; BV, bone volume; CT, computed tomography; DPD, deoxypyridinoline; ES, eroded surface; GIP, gastric inhibitory polypeptide; GLP, glucagon-like peptide; N.Mu.Oc, number of multinuclear osteoclasts; N.Oc, number of osteoclasts; TV, tissue volume; WT, wild type.

***Endocrinology* is published monthly by The Endocrine Society (http://www.endo-society.org), the foremost professional society serving the endocrine community.**

Downloaded from endo.endojournals.org at KYOTO UNIVERSITY on February 28, 2008

contrast to information derived from studies of GIP and GLP-2 on bone formation and resorption, the physiological role of GLP-1, if any, on bone is completely unknown. Because the GLP-1 receptor is expressed in thyroid C cells, and GLP-1 directly stimulates the secretion of calcitonin (10, 11), a potent inhibitor of osteoclastic bone resorption, GLP-1 may contribute to nutrient-mediated reduction of bone resorption.

In the present study, we have investigated the role of endogenous GLP-1 in the regulation of bone metabolism using GLP-1 receptor knockout (Glp-1r$^{-/-}$) mice. We performed morphological analyses of bones from Glp-1r$^{-/-}$ mice and wild-type (WT) littermate controls, including densitometry and histomorphometry. We also evaluated the effects of exogenous GLP-1 on thyroid C cells, and we determined the effect of calcitonin treatment in Glp-1r$^{-/-}$ mice. Taken together, our data illustrate an essential role for the GLP-1 receptor in the control of bone resorption.

Materials and Methods

Animals

Glp-1r$^{-/-}$ mice and Glp-1r$^{+/+}$ littermate WT controls were maintained on a C57BL/6 background as described previously (12). Mice were kept in cages with four to six animals per cage with free access to standard rodent diet and water. Male mice were used for all experiments. Crown to rump length was measured from tip of the nose to the end of the body. All procedures for animal care were approved by the Animal Care Committee of Kyoto University Graduate School of Medicine.

Bone densitometry and body composition analysis

For computed tomography (CT)-based analysis of bone mineral density (BMD), 10-wk-old WT and Glp-1r$^{-/-}$ mice were anesthetized with ip injections of pentobarbital sodium (Nembutal; Dainippon Pharmaceutical, Osaka, Japan). Tibiae (between proximal and distal epiphysis) and lumber spines (between L2 and L4) were scanned at 1-mm intervals using an experimental animal CT system (LaTheta LCT-100; Aloka, Tokyo, Japan). Bone mineral content (BMC) (milligrams), bone volume (cubic centimeters), and BMD (milligrams per cubic centimeter) were calculated using the LaTheta software (version 1.00). The minimum moment of inertia of cross-sectional areas (milligram-centimeters), which represents the flexural rigidity, and the polar moment of inertia of cross sectional areas (milligram-centimeters), which represents the torsional rigidity, were also calculated automatically by the LaTheta software (13). For body composition analysis, the whole bodies of 10-wk-old WT and Glp-1r$^{-/-}$ mice were scanned using the LaTheta CT system.

Bone histomorphometry

Six-week-old male mice were used for studies of bone histomorphometry as described previously (2). Briefly, mice were double labeled with sc injections of 30 mg/kg tetracycline hydrochloride (Sigma Chemical Co., St. Louis, MO) 4 d before being killed and 10 mg/kg calcein (Dojindo Co., Kumamoto, Japan) 2 d before being killed. Bones were stained with Villanueva bone stain for 7 d, dehydrated in graded concentrations of ethanol, and embedded in methyl-methacrylate (Wako Chemicals, Osaka, Japan) without decalcification. Bone histomorphometric measurements were made using a semiautomatic image analyzing system (System Supply, Ina, Japan) and a fluorescent microscope (Optiphot; Nikon, Tokyo, Japan) set at a magnification of ×400. Standard bone histomorphometrical nomenclatures, symbols, and units were used as described in the report of the American Society of Bone and Mineral Research Histomorphometry Nomenclature Committee (14).

Osteoclast and osteoblast assays

For osteoclast differentiation assay, mouse primary osteoblasts and bone marrow cells were cocultured for 7 d in α-MEM (Sigma) containing 10% fetal bovine serum in the presence or absence of 10^{-8} M 1α,25-dihydroxyvitamin D_3 with or without 10^{-5} M GLP-1 (Peptide Institute, Inc., Osaka, Japan). Cells positively stained for tartrate-resistant acid phosphatase containing more than three nuclei were counted as osteoclasts (15, 16). For pit formation assay of mature osteoclasts (16), aliquots of crude osteoclast preparations were plated on dentine slices and cultured with or without 10^{-4} M GLP-1 or 10^{-10} M calcitonin (Peptide Institute) for 48 h. The number of resorption pits was quantified under scanning electron microscopy. For osteoblast apoptosis assay, Saos-2 osteoblasts (Dainippon Pharmaceutical Co., Ltd., Osaka, Japan) were pretreated for 1 h with or without 10^{-6} M GLP-1 and then incubated for an additional 6 h in the presence or absence of 50 μM etoposide, as described previously (2).

Biochemical measurements

Total calcium concentration was measured using Spotchem SP-4420 (Arkray, Kyoto, Japan), and ionized calcium was measured using a blood gas analyzer (GEM premier 3000; Instrumentation Laboratory, Tokyo, Japan) after overnight fasting and 6 h after refeeding. Plasma insulin, leptin, and intact PTH levels were determined by ELISA kits for mouse insulin (Shibayagi, Gunma, Japan), mouse leptin (Morinaga, Yokohama, Japan) and mouse intact PTH (Immutopics Inc., San Clemente, CA). Urinary deoxypyridinoline (DPD) concentrations were measured using an ELISA kit (Quidel, San Diego, CA) before and at 4 h after single administration of 10 IU/kg eel calcitonin (Elcitonin; Asahi Kasei Pharma, Tokyo, Japan).

RNA preparation and quantitative real-time PCR

For analysis of thyroid calcitonin gene expression, mice were injected ip with the GLP-1 receptor agonist exendin-4 (Sigma) at a dose of 24 nmol/kg or the same volume of PBS 6 h before RNA isolation. Total RNA was extracted from thyroid tissue using RNeasy Mini Kit (QIAGEN, Valencia, CA). cDNAs were synthesized by SuperScript II Reverse Transcriptase system (Invitrogen, Carlsbad, CA) and subjected to quantitative real-time PCR using SYBR Green master kit and the ABI PRISM 7000 Sequence Detection System (Applied Biosystems, Foster City, CA). Primers for the calcitonin gene were calcitonin forward 5-CTCACCAG-GAAGGCATCAT-3 and calcitonin reverse 5- CAGCAGGCGAACTTCT-TCTT-3′. The relative amount of mRNA was calculated with glyceraldehyde-3-phosphate dehydrogenase (GAPDH) mRNA as the invariant control: GAPDH forward 5-TCGTTGATGGCAACAATCTC-3 and GAPDH reverse 5′-AAATGGTGAAGGTCGGTGTG-3.

Statistical analysis

Results are expressed as means ± SE. Statistical significance was assessed by ANOVA and unpaired Student's *t* test, where appropriate. A P value of <0.05 was considered to be statistically significant.

Results

Baseline characteristics of WT and Glp-1r$^{-/-}$ mice

Growth of Glp-1r$^{-/-}$ mice was similar to that of WT mice in body weight during the 50-wk observation period (supplemental Fig. 1A, published as supplemental data on The Endocrine Society's Journals Online web site at http://endo.endojournals.org). Body length and length of tibia measured at 10 and 50 wk of age were also almost identical to each other (supplemental Fig. 1, B and C). No significant difference was observed in fat mass (supplemental Fig. 1D) and lean body mass (supplemental Fig. 1E) between 10-wk-old WT and Glp-1r$^{-/-}$ mice determined by CT-based body composition analysis. Similarly, plasma leptin levels (supplemental Fig. 1F) were comparable in 10-wk-old WT and Glp-1r$^{-/-}$ mice. These data indicate that there was no difference between WT and Glp-1r$^{-/-}$ mice in body mass, body composition, or hormone levels that might affect bone mass.

Downloaded from endo.endojournals.org at KYOTO UNIVERSITY on February 28, 2008

Decreased cortical bone mass and diminished bone rigidity in the tibia of Glp-1r$^{-/-}$ mice

To evaluate the impact of the lack of GLP-1 receptor signaling on bone mass, we performed CT-based bone densitometry in bones of differing cortical/cancellous bone ratio. Tibia and lumber spine were used because the former has a higher cortical/cancellous bone ratio, whereas the latter has a lower cortical/cancellous bone ratio. The results are shown as total, cortical, cancellous, and trabecular bone mass in Fig. 1. There was no significant difference between WT and Glp-1r$^{-/-}$ mice in BMC (milligrams) (Fig. 1, A–D) and bone volume (cubic centimeters) (Fig. 1, E–H). Total BMD of tibia was significantly lower in Glp-1r$^{-/-}$ mice than in WT mice (WT mice, 612.97 ± 4.03 mg/cm^3; Glp-1r$^{-/-}$ mice, 570.07 ± 4.22 mg/cm^3; $P = 0.0000036$), but no significant difference was observed in total BMD of spine (Fig. 2I). Cortical BMD also was significantly decreased in Glp-1r$^{-/-}$ mice compared with WT mice in both tibia and spine (tibia: WT mice, 687.34 ± 3.57 mg/cm^3; Glp-1r$^{-/-}$ mice, 650.06 ± 10.59 mg/cm^3; $P = 0.0093$; spine: WT mice, 411.31 ± 8.77 mg/cm^3; Glp-1r$^{-/-}$ mice, 380.45 ± 6.67 mg/cm^3; $P = 0.018$) (Fig. 1J). However, cancellous and trabecular BMD were not significantly different in WT and Glp-1r$^{-/-}$ mice in both tibia and spine (Fig. 1, K and L). Reflecting the loss of cortical bone, Glp-1r$^{-/-}$ mice showed skeletal fragility by diminished bone rigidity indexes. The minimum moment of inertia of cross-sectional areas, which represents flexural rigidity, was significantly reduced in Glp-1r$^{-/-}$ mice (WT mice, 0.014 ± 0.002 mg·cm; Glp-1r$^{-/-}$ mice, 0.008 ± 0.001 mg·cm; $P = 0.022$) (Fig. 1M). Moreover, torsional rigidity as indicated by the polar moment of inertia of cross-sectional areas also was significantly diminished in Glp-1r$^{-/-}$ mice (WT mice, 0.064 ± 0.006 mg·cm; Glp-1r$^{-/-}$ mice, 0.040 ± 0.006 mg·cm; $P = 0.020$) (Fig. 1N). These results indicate that Glp-1r$^{-/-}$ mice have cortical osteopenia and bone fragility.

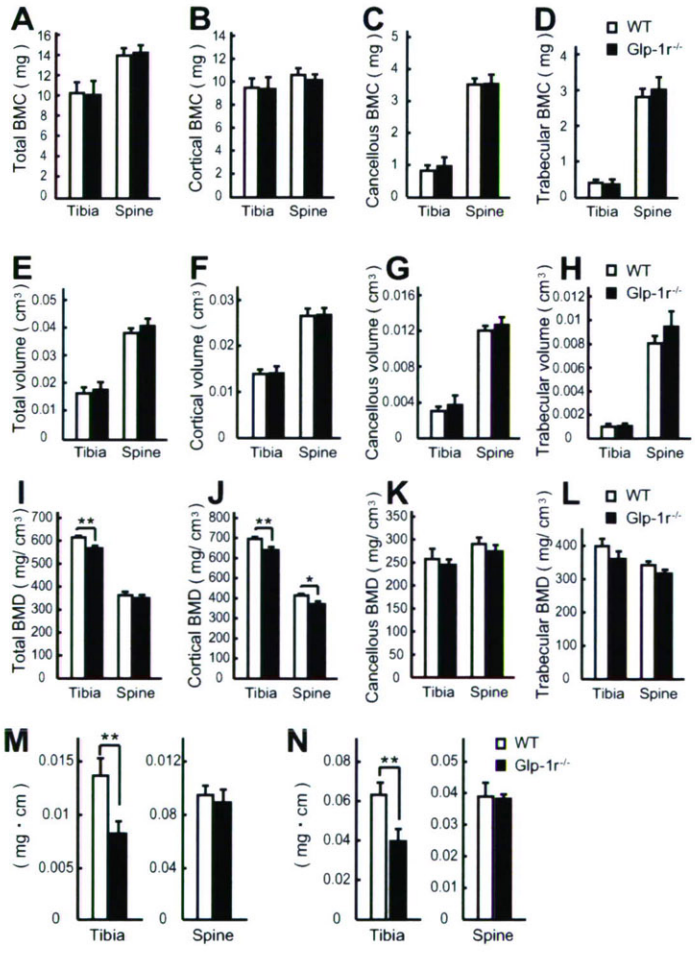

FIG. 1. CT-based bone densitometry of tibia and lumbar spine in 10-wk-old male WT (*white bars*) and Glp-1r$^{-/-}$ (*black bars*) mice. A–D, Total (A), cortical (B), cancellous (C), and trabecular (D) BMC; E–H, total (E), cortical (F), cancellous (G), and trabecular (H) BV; I–L, total (I), cortical (J), cancellous (K), and trabecular (L) BMD; M, minimum moment of inertia of cross-sectional areas, representing the flexural rigidity; N, the polar moment of inertia of cross-sectional areas, representing the torsional rigidity, calculated by LaTheta software. Values are expressed as means ± SE; n = 6 mice per group. *, $P < 0.05$; **, $P < 0.01$, WT *vs.* Glp-1r$^{-/-}$ mice.

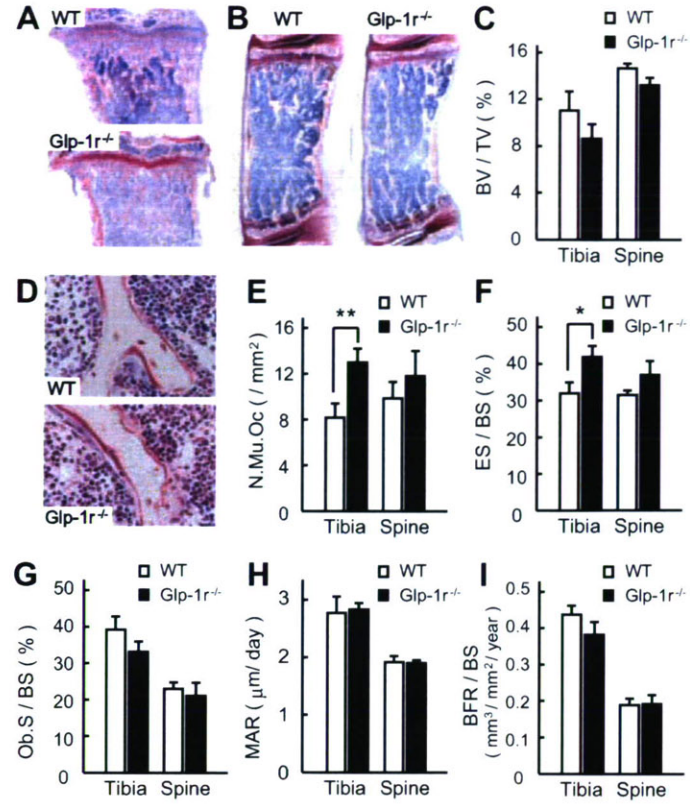

FIG. 2. Bone histomorphometry of tibia and lumbar spine in 6-wk-old male WT (*white bars*) and Glp-1r$^{-/-}$ (*black bars*) mice. A, Representative pictures of proximal tibia. Original magnification, ×20. B, Representative pictures of lumbar spine. Original magnification, ×40. C, BV/TV of tibia and lumbar spine in WT and Glp-1r$^{-/-}$ mice. D, Multinuclear osteoclasts in WT and Glp-1r$^{-/-}$ mice. Original magnification, ×400. E and F, N.Mu.Oc (E) and ES/BS (F) as cellular activity parameters regarding bone resorption. G–I, Osteoblast surface (Ob.S)/BS (G), mineral apposition rate (MAR) (H), and bone formation rate (BFR)/BS (I) as bone formation parameters. Values are expressed as means ± SE; n = 5–7 mice per group. *, $P < 0.05$; **, $P < 0.01$, WT *vs.* Glp-1r$^{-/-}$ mice.

Glp-1r$^{-/-}$ mice exhibit increased numbers of osteoclasts and bone resorption activity in the tibiae

We next performed histomorphometrical analyses of proximal tibiae (Fig. 2A) and lumbar spines (Fig. 2B) of 6-wk-old

Downloaded from endo.endojournals.org at KYOTO UNIVERSITY on February 28, 2008